

On the Transferability of Visual Features in Generalized Zero-Shot Learning

Paola Cascante-Bonilla[†] Leonid Karlinsky[‡] James Seale Smith[§] Yanjun Qi[‡] Vicente Ordonez[†]
[†]Rice University [‡]MIT-IBM Watson AI Lab [§]Georgia Institute of Technology [‡]University of Virginia
 {pc51, vicenteor}@rice.com, leonidka@ibm.com, jamessealesmith@gatech.edu, yq2h@virginia.edu

Abstract

Generalized Zero-Shot Learning (GZSL) aims to train a classifier that can generalize to unseen classes, using a set of attributes as auxiliary information, and the visual features extracted from a pre-trained convolutional neural network. While recent GZSL methods have explored various techniques to leverage the capacity of these features, there has been an extensive growth of representation learning techniques that remain under-explored. In this work, we investigate the utility of different GZSL methods when using different feature extractors, and examine how these models' pre-training objectives, datasets, and architecture design affect their feature representation ability. Our results indicate that 1) methods using generative components for GZSL provide more advantages when using recent feature extractors; 2) feature extractors pre-trained using self-supervised learning objectives combined with cross-entropy and knowledge distillation provide better feature representations, increasing up to 15% performance when used with recent GZSL techniques; 3) specific feature extractors pre-trained with larger datasets do not necessarily boost the performance of GZSL methods. In addition, we investigate how GZSL methods fare against CLIP, a more recent multi-modal pre-trained model with strong zero-shot performance. We found that GZSL tasks still benefit from generative-based GZSL methods along with CLIP's internet-scale pre-training to achieve state-of-the-art performance in fine-grained datasets. We release a modular framework for analyzing representation learning issues in GZSL here: <https://github.com/uvavision/TV-GZSL>.

1. Introduction

Deep learning models have achieved remarkable accuracy in many computer vision classification tasks when labeled data is available, and the data distribution is consistent during training and test time [19, 35, 43]. It is now possible to train image classifiers that can distinguish with high accuracy thousands of image categories [37]. However, in order to enable a model to recognize novel categories, it is still necessary to collect a dataset with representative human-labeled

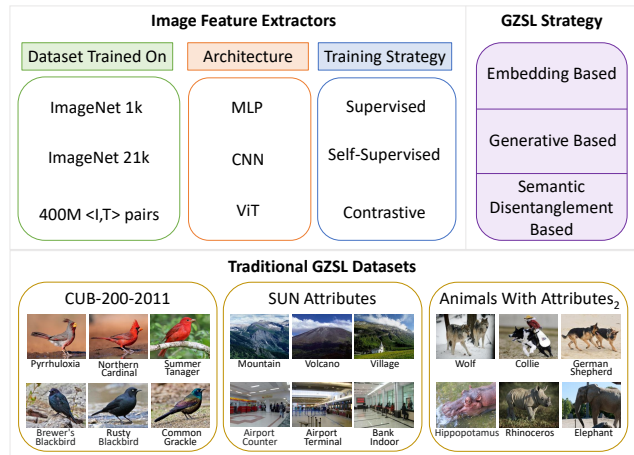


Figure 1. **Overview of our large-scale analysis.** We explore a diverse set of visual feature backbones that were trained using different objectives. We further use them to extract visual features and train a diverse set of classic and modern Generalized Zero-shot Learning (GZSL) methods. We use three standard datasets to measure the methods' performance: CUB-200-2011 and SUN Attributes, which are fine-grained, and Animals with Attributes 2 (AWA2) which is a coarse-grained dataset. Best viewed in color.

examples. For this reason, literature has proposed zero-shot learning to help a model recognize novel *unseen* categories without needing any images of the new category. Zero-shot learning relies on auxiliary information such as textual descriptions or category attributes [14, 15, 28]. The general idea is to leverage the auxiliary information to transfer visual knowledge from images in *seen* categories to a set of images from *unseen* categories. Once this function is learned, it can be used to categorize *unseen* samples into novel classes.

Early work on zero-shot learning focused on obtaining a good accuracy just on a set of *unseen* categories at inference time. In a more challenging scenario known as Generalized Zero-shot Learning (GZSL), both *seen* and *unseen* categories are considered at test time [6, 32]. This setup is more realistic and has been adopted in all the recent works in zero-shot learning; therefore, we focus exclusively on this setting.

First-generation methods are coined as embedding-based techniques, which focus on learning a function to align the

seen images and unseen attributes and further measure the similarity between the mapped and predicted representations of the data samples in the embedding space [3, 36, 51, 52]. Further GZSL methods have shown significant improvement over this early work by teaching a model to generate the visual features of the *unseen* classes based on the visual features of the *seen* classes and the semantic representations of both *seen* and *unseen* categories. More recent works have instead explored rich image feature representations and their ability to provide enough information for a mapping function to generalize to new classes [9, 46]. These methods propose to learn discriminative representations from image features through disentanglement over feature groups by factorizing the useful dimensions to avoid bias towards the seen categories when trying to learn an attribute-visual alignment.

While disentanglement-based methods have significantly improved over prior work, the representation capabilities of image features have mostly been tested under a ResNet101 model [22] pre-trained on Imagenet [29, 50]. In this work, we propose to explore different architectures trained with different objectives to be used as feature extractors. Given the wide availability of pre-trained model parameters [2, 10, 17], we perform a large-scale analysis to assess the impact of modern visual features backbones, our results are summarized in Figure 1. In our analysis, we consider visual features extracted from both uni-modal and multi-modal architectures pre-trained on standard settings, i.e., models pre-trained with ImageNet-1K; to models pretrained with even larger amounts of data, i.e., models pre-trained with ImageNet-21K and models pre-trained with 400 million Image/Text pairs.

Our results show that ResNet101 and similar feature extractors may not provide enough information, given the nature of the backbone architecture limitations and the training objective. Moreover, when examining feature extractors pre-trained with larger datasets, one would assume that the features extracted would contain more similarities to the data present in the GSZL test splits, causing all methods to perform better due to data leakage. However, we found that using features extracted from large-scale pre-trained *uni-modal networks* does not significantly impact the zero-shot performance. Our experiments also reveal that with feature representations extracted from Visual Transformer [12] based architectures, no semantic disentanglement module is necessary to achieve state-of-the-art performance, and generative-based methods are superior in all benchmarks by a large margin ($\approx 23\%$) when using features extracted from Transformer based architectures [12] trained with a contrastive objective. Furthermore, given the capabilities of new models [23, 33, 41] to generalize to new tasks, we investigate how CLIP [33] performs against GZSL methods and reveal that generative-based GZSL techniques are still necessary to achieve state-of-the-art results on fine-grained datasets.

Our primary contributions can be summarized as follows:

- A large-scale study of different methods and features extracted from a diverse set of architectures and training approaches, applied to state-of-the-art methods from different GZSL families (i.e., embedding based [3, 16, 36], generative based [20, 30, 38], semantic disentanglement based [8, 9, 46]).
- A library containing the revisited GSZL methods we chose to explore, allowing a unified codebase for reproducibility and further analysis based on the findings shown in this work. Texts generated to finetune the models based on the attribute vectors provided in each dataset, along with the weights and the extracted features we use in our experiments.
- Updates and key insights which we hope will reshape the Generalized Zero-Shot Learning research track in favor of leveraging richer feature representations.

We expect our work to motivate further feature representation explorations to the GZSL task in a more realistic, practical, and challenging scenario, given the recent advances with large pre-trained models. All the resources used, including GPU information and computing infrastructure are detailed in the Appendix, along with hyperparameter selections and data splits we use for all our experiments.

2. Related Work

The goal of GZSL is to classify images from both seen and unseen categories by transferring knowledge from seen to unseen classes using a set of attributes as auxiliary information. Since every attribute vector entry represents a class description, the assumption is that the classes with similar descriptions contain a similar attribute vector in the semantic space. Therefore, the general idea is to learn a function that allows this mapping between modalities. The general idea is to align visual features from seen classes with their corresponding attribute vectors. Current methods can be broadly categorized into:

Embedding-based methods, which aim to learn a mapping function or a projection between visual features and their attributes or descriptions [3, 16, 36]. This mapping function is used to project image features into a semantic space so that it is possible to classify seen and unseen classes by estimating how close these features are to a class embedding vector [7, 27, 34, 40].

Generative-based methods, which synthesize an unlimited number of visual features using the auxiliary information from the unseen classes, and compensate for the imbalance classification problem that poses the GZSL task [20, 30, 38]. A generative model is a probabilistic model that is representative of the conditional probability of the observable input X , given a target y [18, 24]. Recent advances in generative modeling have gained a significant amount of attention.

In the GZSL setting, generative models are leveraged to learn to generate visual features or images for the unseen classes [25, 42]. This is achieved using samples from the seen classes and semantic representations of both seen and unseen classes. Generative-based methods convert the GZSL problem into a supervised learning problem by generating samples for both seen and unseen classes.

Semantic disentanglement-based methods, which aim to factorize the useful dimensions of a given visual feature to learn the attribute-visual alignment. The assumption is that the image features extracted from a ResNet101 that was pre-trained on Imagenet, broadly used in all traditional GSZL datasets [31, 49, 50], are not ideal for the zero-shot learning task [8, 9, 46]. Since these features are not representative with respect to the specific attributes that describe the image parts/composition, not all the dimensions of these features are semantically related to the given attributes; thus, it is necessary to factorize or disentangle the useful dimensions to avoid bias when trying to learn the attribute-visual alignment. In this context, entanglement refers to the property of not having independence among attributes of one representation. In an entangled representation, all the factors of variation are mixed, and there is no explicit separation that represents the important characteristics in the images [4]. On the other hand, given an image dataset of birds such as the CUB dataset [49], a disentangled representation may consist of separate dimensions for wing color, breast color, bill shape, tail pattern, crown color, wing pattern, etc [13].

3. Generalized Zero-Shot Learning

In the GZSL setting, we define S as the set of seen classes within N_s categories and Y_s as their corresponding labels. We also define U as the set of unseen classes with N_u categories and Y_u as their corresponding labels. Here, S and U have no intersection. Each set consists of image-features x , class labels y available during training and class-embeddings $c(y)$. Thus, $S = \{x_i^s, y_i^s\}_{i=1}^{N_s}$ and $U = \{x_i^u, y_i^u\}_{i=1}^{N_u}$. Additionally, we have access to a set of semantic descriptions of the seen and unseen classes $A = \{a_i^s\}_{i=1}^{N_s+N_u}$, which are typically class-embeddings vectors of hand-annotated attributes. The image features are typically extracted from a feature backbone (i.e. ResNet101 pretrained on ImageNet-1K). When training, we use A along with the visual features and labels from the seen set (i.e., $\{x_i^s, y_i^s\}_{i=1}^{N_s}$) and only the labels from the unseen set (i.e., $\{y_i^u\}_{i=1}^{N_u}$). Finally, the test set contains image-features from both S and U , and their corresponding labels. This section presents and describes all the methods we include in this study grouped by their corresponding family of methods. These can be characterized as: embedding-based, generative-based and disentanglement-based. We also present all the datasets we use in our study. Additional training and computational details are included in the Appendix.

3.1. Embedding-based Methods

DeViSE: A Deep Visual-Semantic Embedding Model [16] (2013) propose to learn a linear mapping between the image and the semantic space and introduce the use of a ranking loss instead of an L_2 loss. This avoids making the vectors become closer to one another without taking into account the incorrect labels that are closer to the target image.

An embarrassingly simple approach to zero-shot learning (ESZSL) [36] (2015) use a linear model to create relationships between features, attributes and classes. This linear model has two layers, the first layer helps in defining the relationship between features and attributes, and the second layer deals with modeling the relationship between attributes and classes where the prescribed attribute signatures are fixed. This method uses a square loss to learn the bilinear compatibility between attributes and their corresponding classes.

Label-Embedding for Image Classification present an *Attribute Label Embedding approach (ALE)* [3] (2016), they propose to embed each class in the space of attribute vectors, and further propose to learn a bilinear compatibility function between the image and a label embedding using a ranking objective function.

3.2. Generative-based Methods

Generalized Zero- and Few-Shot Learning via Aligned Variational Autoencoders (CADA-VAE) [38] (2019) use two variational autoencoders (VAEs [24]) to align the visual and semantic features by learning a shared latent space between both modalities. Then, these VAEs are used to synthesize a large number of seen and unseen features, which are then used to train a classifier.

Latent Embedding Feedback and Discriminative Features for Zero-Shot Classification (tfVAEGAN) [30] (2020) propose to use a feedback module in a model that combines a variational autoencoder (VAE [24]) and a generative adversarial network (GAN [18]) to modulate the latent representation of the generator. They propose to enforce semantic consistency by introducing a feedback loop from the semantic embedding decoder. They propose to use both synthesized features and latent embeddings during classification.

More recently, hybrid methods such as *Contrastive Embedding for Generalized Zero-Shot Learning (CE)* [20] (2021) have emerged. This method proposes to integrate the generation model with the embedding model to map the real and the synthetic samples produced by the generation model into an embedding space. To do this, they leverage a contrastive loss that learns to discriminate between one positive sample and a large number of negative samples from different semantic descriptor classes. They claim that the original visual feature space is suboptimal for GZSL classification since it lacks discriminative information, which they aim to learn using the contrastive objective.

3.3. Semantic Disentanglement-based Methods

FREE: Feature Refinement for Generalized Zero-Shot Learning [8] (2021) use a feature refinement module to jointly map the semantic and visual modalities, and refine the visual features of seen and unseen class samples – dropping unnecessary information from the visual features. They use the class label supervision and a semantic cycle-consistency constraint to guide the proposed module to learn relevant feature representations that are also semantically relevant with respect to their corresponding classes.

Semantics Disentangling for Generalized Zero-Shot Learning (SDGZSL) [9] (2021) introduce a total correlation penalty that is applied to the visual features of unseen classes that were generated by a conditional VAE [24]. This work uses a Relation Network [44] to correlate the factorized estimated features – the *semantic-consistent* and the *semantic-unrelated* latent features.

3.4. GZSL Datasets

We use three datasets. *Caltech-UCSD Birds-200-2011 (CUB)* [49], a fine-grained dataset with 11,788 images from 200 different types of birds annotated corresponding to 150 seen and 50 unseen classes, with 312 attributes. *SUN Attribute (SUN)* [31], a fine-grained dataset with 14,340 images from 717 types of scenes corresponding to 645 seen and 72 unseen classes, annotated with 102 attributes. *Animals with Attributes2 (AWA2)* [50], a dataset with 37,322 images from 50 animal classes corresponding to 40 seen and 10 unseen classes, annotated with 85 attributes. We report the *seen* and *unseen* accuracy, and their harmonic mean.

4. Pre-Trained Image Feature Extractors

We begin our analysis by extracting the corresponding image features for all our samples using a diverse set of popular models pre-trained on Imagenet-1k and Imagenet-21k – whose weights are publicly available. Prior work [50] mention that using GoogLeNet features is not as effective as using Resnet101 features; thus, we want to further investigate: does feature extractor size matters for GZSL? This work aims to evaluate if pre-training on a bigger set impacts the outcomes, and if similarly robust features extracted from different model architectures – other than Resnet101 – makes a significant difference. For the backbones that were pre-trained using Imagenet-1k, we make sure that we use the same splits proposed in [50] so that pre-trained features do not violate the zero-shot principle. We also want to measure the impact of using visual features extracted from networks that were pre-trained with data present in the test set of our settings. Thus, we investigate how the selected GZSL methods leverage the information extracted from larger backbones pre-trained with bigger and more diverse datasets (i.e., Imagenet-21k).

4.1. Unimodal Feature Backbones

Overall, the pool of networks in this study have been trained using two learning objectives: *Supervised Learning* (SL), which aims to learn a function that maps an input to a *known output*, and is typically trained using a *cross-entropy* loss (e.g., Resnet101 [22]) or *distillation* (e.g., DeiT [47]). On the other hand, *Self-Supervised Learning* (SSL), aims to learn a function that maps an input to a *unknown output*; SSL can be accomplished using a *contrastive loss* such as InfoNCE (e.g., MoCo [21]) or adding *distillation* along with a similarity metric measured with a cross-entropy loss applied over the features of two different random transformations of an input image (e.g., DINO [5]). We perform experiments on three broad types of unimodal architectures trained on images only (Imagenet-1k or Imagenet-21k): *Convolutional Neural Networks* (CNN) [26] trained using the images as a whole under SL or SSL, *Vision Transformers* (ViT) [12] which takes an image, transforms it in a sequence of image patches and is trained using either SL or SSL; and *Multi-Layer Perceptron Mixers* (MLP) [45] which also exploit image patches and are trained with supervision.

We chose the most performant models and fine-tuned them using only the training samples from the seen classes. Since the visual features are extracted from a diverse set of architectures trained in the wild, we focus on the *inductive* setting, where there is no access to the unlabeled visual data from the unseen classes. In this way, we mitigate any bias reinforced by additional training of the visual representations. This practice has been followed to achieve better results in prior literature (which only uses Resnet101 features); however, there are no available reports for all the methods using these features; thus, we run all methods and report our findings in Section 5.

4.2. Multimodal Feature Backbones

In addition, we study CLIP [33], a multi-modal model with a visual encoder and a textual encoder trained with 400 million image/text pairs in a contrastive way. Traditionally, all GZSL methods disregard the attribute values as they are given for granted, and no additional analysis is performed. We instead take a closer look at these semantic features and their corresponding attributes (e.g., color, shape, type of animal, type of place, etc) and use them to fine-tune several pre-trained CLIP models.

We perform three experiments with CLIP: (A) We directly evaluate the model using the images and class names without any further pre-training or post-processing by directly looking at the ranking the model yields for each seen and unseen samples, (B) We fine-tune CLIP using the class names, the attribute values and a combination of class names + attribute values, and evaluate its performance, (C) We extract the visual features from the CNN and ViT based visual backbones available in their public repository, and use the features ex-

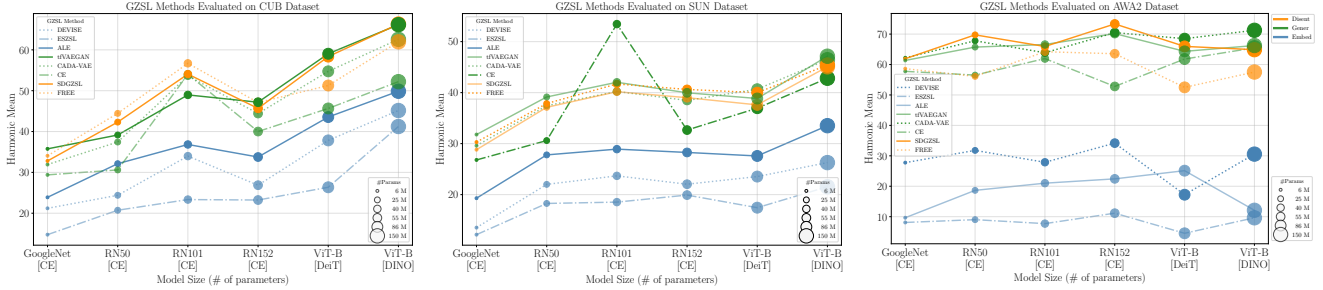


Figure 2. **Impact of Model Parameter Size.** We show the Harmonic Mean performance of different methods when using a specific model to extract the features of image samples from CUB, SUN, and AWA2 datasets. All models were pre-trained using ImageNet-1k. The blue lines correspond to the embedding-based methods, the green lines correspond to the generative-based methods, and the orange lines correspond to the semantic disentanglement-based methods. Best viewed in color.

tracted from (A) and (B) to train the GZSL methods. We go over our findings in Section 6.

5. Results using Unimodal Feature Extractors

We evaluate all GZSL methods trained with feature extractors pre-trained using ImageNet-1k. In Figure 2, we show the Harmonic Mean performance of different methods when using a specific model to extract the features of image samples. Surprisingly, CADA-VAE [38] and tfVAEGAN [30] consistently outperform all methods. While current disentanglement methods show significant improvements when using features from transformer-based architectures, they are outperformed by the generative-based methods. We can also observe that DINO [5] provides better feature representations for all methods across all datasets.

We also want to evaluate the impact of using a feature extractor with the *same architecture type but trained with different learning objectives*. In Figure 3, we show the Harmonic Mean performance of different GZSL methods when using a Resnet model architecture pre-trained on Imagenet-1k as the image feature extractor. Surprisingly, the features extracted from DINO [5] increase the Harmonic Mean per-

formance up to 15% in both fine-grained datasets (i.e., CUB and SUN datasets). More surprisingly, the feature vectors extracted from MOCO perform worse than traditional supervised learning models trained with a cross-entropy objective function. MOCO’s training objective is formulated by the InfoNCE loss, which encourages the model to maximize the Mutual Information (MI) between N random samples containing one positive sample, and minimize the Mutual information between the anchor sample and $N - 1$ negative samples. On the other hand, in DINO, a teacher and a student model are trained by feeding two different random transformations of an input image to each network; the objective is to maximize the similarity between both outputs, which is encouraged and measured with a cross-entropy loss. Thus, the generalization capabilities shown with DINO support prior observations when using its image features in classification tasks with respect to other self-supervised techniques [5].

We then evaluate the impact of using feature extractors that were pre-trained with more data variety and size and summarize our findings in Figure 4. Surprisingly, features extracted from backbones trained with more data (Imagenet-21k) do not always perform better, but features extracted

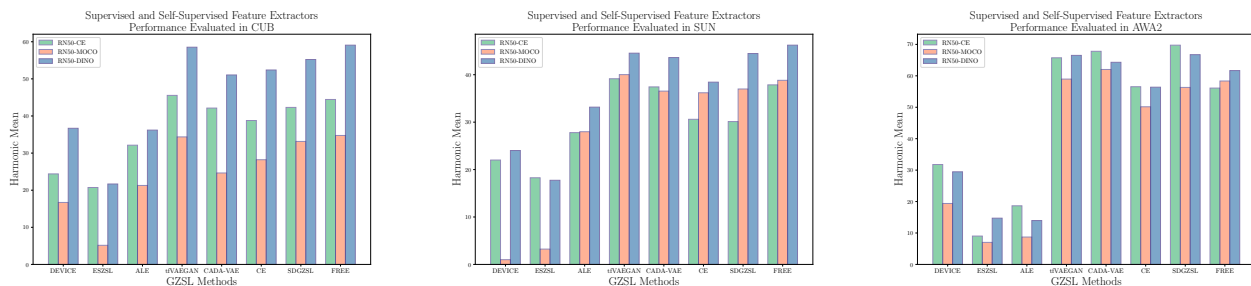


Figure 3. **Same Feature Extractor Pretrained with Different Learning Objectives.** We show the Harmonic Mean performance of different GZSL methods when using a RN50 model to extract the features of image samples from all datasets. RN50-CE indicates that the model was pretrained using categorical cross-entropy in a supervised way, otherwise it was a model pretrained in a self-supervised way using a contrastive loss (RN50-MOCO [21] and RN50-DINO [5]). All these models were pretrained using ImageNet-1k. Best viewed in color.

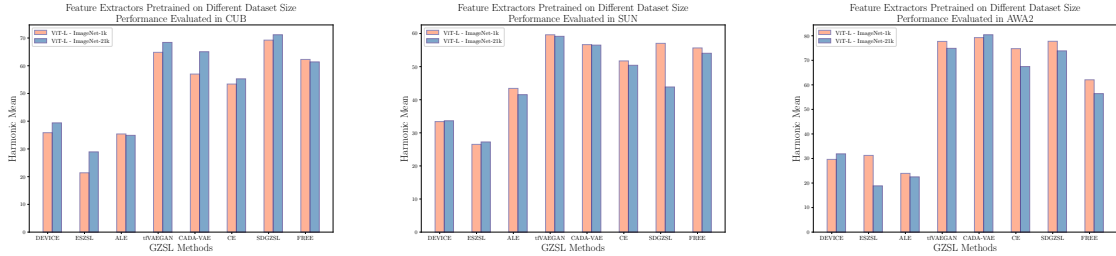


Figure 4. **Same Feature Extractor Pretrained with Different Datasets.** We show the Harmonic Mean performance of different GZSL methods when using a ViT_{Large} model to extract the features of image samples from all datasets. [ViT-L - ImageNet-1k] and [ViT-L - ImageNet-21k] indicates the dataset the model was pretrained with. Best viewed in color.

from bigger architectures seem consistently better.

We show more detailed results on CUB, SUN and AWA2 using GZSL methods grouped in their corresponding families in the following subsections. Please refer to the Appendix to check the full list of numerical results for all unimodal backbones and GZSL methods.

5.1. Results of Embedding-based Methods

The ViT_{huge} features pre-trained on ImageNet-21k seem to be the best for all the methods using ALE. However, for the AWA2 dataset, all methods perform better using the features extracted from a network pre-trained using ImageNet-1k. For CUB and SUN datasets, the performance gap against the features extracted from a network trained using ImageNet-1k and ImageNet-21k is not significant for all methods. More detailed results are available in Tables 6, 7 and 8 from Section D in the Appendix.

5.2. Results of Generative-based Methods

The most performant visual features are extracted from a ViT_{huge} pretrained on ImageNet-21k and fine-tuned with the

seen classes, using the CADA-VAE method. More interestingly, the features from a ViT_{large} pretrained on ImageNet-1k seem competitive with the features from a ViT_{large} pretrained on ImageNet-21k for the CE and tVAEGAN methods respectively. More detailed results are available in Tables 9, 10 and 11 from Section D in the Appendix.

5.3. Results of Disentanglement-based Methods

The most performant visual features are extracted from a ViT_{large} pre-trained on ImageNet-1k using the SDGZSL method. Here, the features extracted from architectures pre-trained using ImageNet-21k perform worse than the ones pre-trained using ImageNet-1k, except for the CUB dataset. More detailed results are available in Tables 12, 13 and 14 from Section D in the Appendix.

6. Results using CLIP as a Multimodal Feature Extractor

Direct evaluation of CLIP using the images and class names without any further pre-training or post-processing: we use different template captions to generate the textual

Backbone	CUB			SUN			AWA2		
	Seen	Novel	Harm.	Seen	Novel	Harm.	Seen	Novel	Harm.
RN50	45.90	45.44	45.67	44.61	48.96	46.68	87.86	82.48	85.08
RN101	48.86	49.44	49.15	45.16	49.24	47.11	88.66	84.79	86.67
RN50x4	51.89	55.27	53.53	48.53	50.56	49.52	92.09	86.52	89.22
RN50x16	56.82	55.19	55.99	49.07	54.44	51.62	94.36	89.11	91.65
RN50x64	63.81	57.19	60.32	55.28	51.59	53.37	95.11	90.11	92.54
ViTB32	51.35	49.65	50.49	48.26	50.97	49.58	90.99	85.69	88.26
ViTB32 [†]	61.46	58.09	59.73	50.66	53.75	52.16	87.84	82.12	84.88
ViTB16	55.76	56.23	55.99	50.97	56.11	53.42	93.68	87.19	90.32
ViTL14	62.62	63.19	62.90	55.97	58.06	56.99	95.80	89.39	92.48
ViTL14 [†]	64.45	62.69	63.56	57.79	62.64	60.12	96.06	89.91	92.88

Table 1. Results of using publicly available pre-trained CLIP [33] models with different backbones to evaluate three standard GZSL datasets. [†] indicates we used a set of captions similar to the proposed by OpenAI to test on Imagenet [11], [†] indicates the model used was trained on the Laion400M [39] dataset.

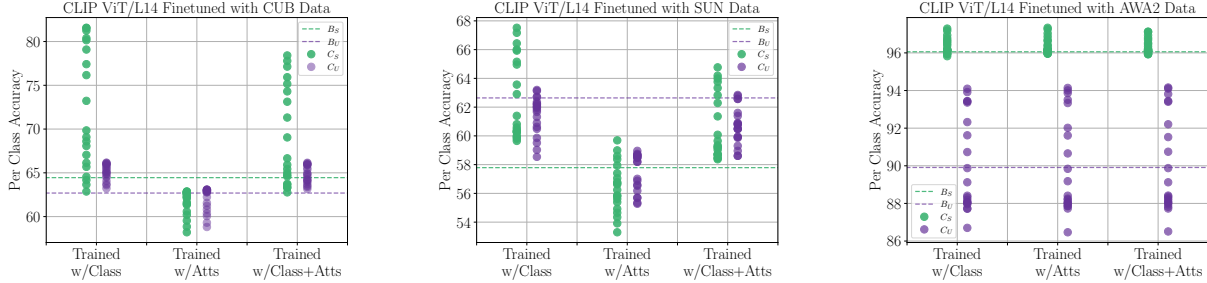


Figure 5. **Fine-tuning CLIP with seen samples.** Results of fine-tuning a CLIP model using the images and different text descriptions, including the class name, the attribute text, and combining both text captions. We show accuracy variations after 110k training iterations for CUB [49], SUN [31] and AWA2 [50], where B_S and B_U indicate the base performance of seen and unseen classes without fine-tuning. C_S refers to the seen classes, and C_U refers to the unseen (novel) classes after fine-tuning.

descriptions (e.g., "An image of a [class name]") and chose to evaluate the best-performing model with the template captions proposed by OpenAI to test on Imagenet [1]. We also evaluate a CLIP model trained with the publicly available LAION-400M dataset [39] in the publicly available visual transformer backbone (i.e. ViTB32). We show results in Table 1. Overall, we expected CLIP to perform well in all the selected datasets, even with CUB, whose class names are particularly specific; similar results on this dataset have been reported in concurrent work [48]. Moreover, our results

show that generative-based models work on par and even outperform CLIP when using the Resnet101 fine-tuned features, indicating that there might be room for improvement.

Evaluation of CLIP performance after fine-tuning using the class names, the attribute values and a combination of class names & attribute values: Figure 5 shows the accuracy variations after fine-tuning CLIP for 110k iterations using different types of text prompts, using only the seen training set for each dataset. Interestingly, we observed that fine-tuning enhances both the seen and unseen accuracy.

GZSL Methods using CLIP Visual Features

Data Back set	bone	tfVAEGAN			CADA-VAE			SDGZSL			FREE			CE		
		Seen	Novel	Harm.	Seen	Novel	Harm.	Seen	Novel	Harm.	Seen	Novel	Harm.	Seen	Novel	Harm.
CUB	R50 _{x64}	82.09	67.93	74.34	75.91	70.84	73.29	74.77	73.70	74.23	68.53	73.47	70.91	59.06	49.52	53.87
	ViT _{L14}	<u>77.67</u>	<u>72.36</u>	<u>74.92</u>	<u>77.90</u>	<u>72.98</u>	<u>75.36</u>	<u>79.50</u>	73.49	<u>76.38</u>	<u>79.05</u>	65.38	<u>71.56</u>	<u>74.04</u>	46.38	57.03
	ViT _{L14} [†]	80.39	72.86	76.44	81.96	71.24	76.22	79.19	74.70	76.88	78.87	65.89	71.80	71.49	48.62	57.88
	ViT _{L14} [‡]	80.73	73.59	76.99	79.51	74.68	77.01	80.40	74.33	77.25	79.47	68.25	73.44	75.12	51.14	60.86
	ViT _{L14} [§]	82.82	72.27	77.18	81.47	75.05	78.13	80.38	75.67	77.96	80.48	67.54	73.45	71.15	56.82	63.18
SUN	R50 _{x64}	57.21	<u>69.79</u>	62.88	59.46	65.63	62.39	57.17	66.60	61.52	<u>60.04</u>	57.78	58.89	50.04	59.10	54.19
	ViT _{L14}	<u>59.84</u>	68.89	<u>64.05</u>	<u>62.11</u>	<u>63.40</u>	<u>63.18</u>	<u>63.57</u>	62.71	<u>63.13</u>	58.18	<u>62.71</u>	<u>60.36</u>	<u>60.16</u>	57.85	<u>58.98</u>
	ViT _{L14} [†]	61.75	70.49	65.83	61.47	65.76	63.54	62.56	64.44	63.49	58.95	62.99	60.90	52.79	64.37	58.01
	ViT _{L14} [‡]	60.93	67.08	63.86	57.95	68.19	62.65	60.08	67.15	63.42	58.37	62.43	60.33	56.78	64.03	60.19
	ViT _{L14} [§]	62.25	70.03	65.91	58.91	66.74	62.58	60.70	67.50	63.92	58.72	63.61	61.07	59.65	60.90	60.27
AWA2	R50 _{x64}	89.69	68.21	77.49	90.54	63.75	75.81	78.67	69.07	73.56	<u>87.60</u>	61.04	71.95	89.95	63.33	74.33
	ViT _{L14}	<u>90.95</u>	69.50	<u>78.70</u>	<u>92.68</u>	68.14	<u>77.99</u>	<u>89.99</u>	68.76	77.91	81.10	<u>65.99</u>	<u>72.77</u>	<u>85.63</u>	<u>71.96</u>	<u>78.20</u>
	ViT _{L14} [†]	91.25	67.77	77.77	90.48	70.07	78.98	89.18	71.40	79.30	81.27	71.56	75.94	85.12	78.02	81.41
	ViT _{L14} [‡]	93.40	72.61	81.70	93.51	73.85	82.53	85.77	74.16	79.54	81.29	65.62	72.62	89.85	64.12	74.84
	ViT _{L14} [§]	89.62	73.56	80.80	93.35	68.14	78.78	91.50	70.33	79.54	81.53	69.84	75.23	90.78	67.96	77.73

Table 2. Results of Generative and Disentanglement Based Methods for the CUB, SUN and AWA2 datasets using different features extracted from different size and architecture of the visual head from diverse CLIP models (i.e., Resnet50 (R50) and Vision Transformer (ViT)). The three bottom rows per section correspond to fine-tuned features using sentences with: † the class names, ‡ the attributes, and § both class names and attributes. The bold numbers correspond to the highest scores per column, the underline numbers correspond to the to the highest scores using features not fine-tuned, and the shaded rows correspond to the most performing image feature per method over all.

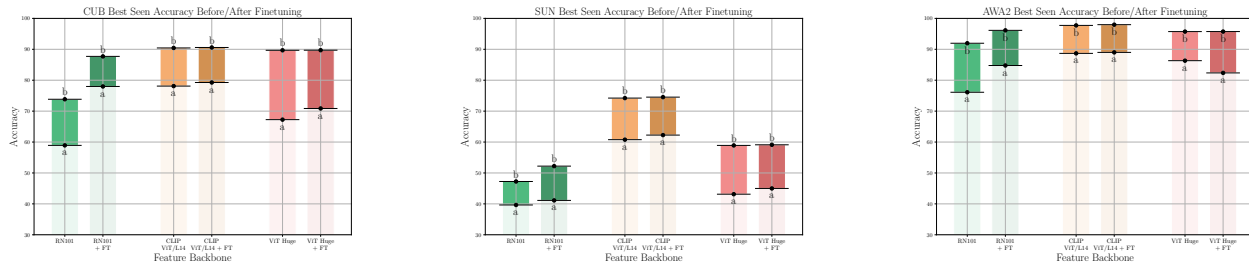


Figure 6. **Fine-tuning diverse feature extractors with seen samples.** We show the difference between: a) the best-seen accuracy achieved among all GZSL methods, and b) the best-seen accuracy after training and evaluating the seen classes using a linear classifier probe. We use different visual features extracted from different backbones and training strategies. The classification upper-bound only increases significantly when fine-tuning the RN101 [22] features but remains the same with the ViT [12] features regardless of the classification objective (i.e., cross-entropy vs. contrastive).

Evaluation of the GZSL methods using the visual features extracted from the visual encoder of CLIP to train all GZSL methods: We show in Table 2 the effect of using CLIP features and which fine-tuned model performs the best. Unsurprisingly, using both class name and class attributes outperforms other backbones. Similarly to uni-modal backbones, the generative-based models (e.g., CADA-VAE and tfVAEGAN) outperform other methods on all datasets. More surprisingly, both methods also outperform the CLIP results in CUB and SUN, but CLIP alone outperforms all methods in the AWA2 dataset. We run experiments using all eight visual encoders available from CLIP model, but show the most relevant results in Table 2. Please refer to the Appendix to check the full list of results.

7. Fine-tuning Feature Extractors

We observe that in the generative and disentanglement-based methods, there seems to be a trade-off in the multi-modal latent space, where some features from the seen set are distilled to the projected features of the unseen set. Typically, these methods augment the training set and convert the problem into a classification task, thus, the final seen accuracy is penalized by the classifier. For this reason, we also investigate how much these models penalize the final accuracy of the seen sets by measuring the difference of a classifier trained only using the seen set versus the best-seen accuracy achieved among all GZSL generative and disentanglement-based methods. The results are shown in Figure 6. We observe that while fine-tuning a Resnet101 model increment the seen accuracy of both the classifier and the GZSL method, it does not increase the seen accuracy of recent models such as vision transformers. We also observe that the seen accuracy of the GZSL method does not improve substantially when using ViT features, and fine-tuning on AWA2 hurts the best seen accuracy on the GZSL result while not improving the classifier seen accuracy.

8. Conclusion

In this paper, we provide strong empirical evidence that indicates that:

- Using Transformer based architectures provides superior feature representation capabilities while not violating the zero-shot principle of being pre-trained on unseen classes.
- The feature representations extracted from unimodal architectures that were pre-trained on larger datasets (e.g., ImageNet-21k) do not necessarily boost GZSL performance.
- Using Convolutional based architectures pre-trained without labels, using contrastive learning and self-distillation, provides better feature representations for GZSL than models trained using supervised learning, with known labels and cross-entropy loss alone.
- Fine-tuning does not significantly impact the performance on Transformer based unimodal backbones but may boost the performance on multimodal backbones.
- Multimodal architectures trained on internet-scale large data (CLIP) still benefit from generative based GZSL methods to achieve state-of-the-art performance in CUB and SUN, which are fine-grained datasets. This may indicate that feature representations from CLIP are more suitable for GZSL when there is less inter-class correlation among data samples.
- Fine-tuning a CLIP model using prompts including the class names and attributes from the seen categories also boosts the ranking performance of the unseen classes.

In summary, our work provides an update on GZSL methods in the era of large-scale multi-modal pre-training, and re-evaluates in this context the progress that has been made so far in this area. We release a well-documented codebase that both replicates our findings and provides a modular framework for further feature representation explorations to the GZSL task with recent large pre-trained models.

Acknowledgements This material is based upon work sup-

ported by the National Science Foundation under Grant No. 2221943 and Grant No. 2201710.

References

- [1] Clip prompt engineering for imagenet. https://github.com/openai/CLIP/blob/main/notebooks/Prompt_Engineering_for_ImageNet.ipynb. Accessed: 2022-06-01. **7**
- [2] Pytorch image models (timm). <https://github.com/rwightman/pytorch-image-models>. Accessed: 2022-06-01. **2**
- [3] Zeynep Akata, Florent Perronnin, Zaïd Harchaoui, and Cordelia Schmid. Label-embedding for image classification. *IEEE Transactions on Pattern Analysis and Machine Intelligence*, 38:1425–1438, 2016. **2, 3, 11, 12**
- [4] Yoshua Bengio, Aaron C. Courville, and Pascal Vincent. Representation learning: A review and new perspectives. *IEEE Transactions on Pattern Analysis and Machine Intelligence*, 35:1798–1828, 2013. **3**
- [5] Mathilde Caron, Hugo Touvron, Ishan Misra, Hervé Jégou, Julien Mairal, Piotr Bojanowski, and Armand Joulin. Emerging properties in self-supervised vision transformers. *2021 IEEE/CVF International Conference on Computer Vision (ICCV)*, pages 9630–9640, 2021. **4, 5**
- [6] Wei-Lun Chao, Soravit Changpinyo, Boqing Gong, and Fei Sha. An empirical study and analysis of generalized zero-shot learning for object recognition in the wild. *ArXiv*, abs/1605.04253, 2016. **1**
- [7] Long Chen, Hanwang Zhang, Jun Xiao, W. Liu, and Shih-Fu Chang. Zero-shot visual recognition using semantics-preserving adversarial embedding networks. *2018 IEEE/CVF Conference on Computer Vision and Pattern Recognition*, pages 1043–1052, 2018. **2**
- [8] Shiming Chen, Wenjie Wang, Beihao Xia, Qinmu Peng, Xinge You, Feng Zheng, and Ling Shao. Free: Feature refinement for generalized zero-shot learning. *2021 IEEE/CVF International Conference on Computer Vision (ICCV)*, pages 122–131, 2021. **2, 3, 4, 11, 12**
- [9] Zhi Chen, Yadan Luo, Ruihong Qiu, Sen Wang, Zi-Yu Huang, Jingjing Li, and Zheng Zhang. Semantics disentangling for generalized zero-shot learning. *2021 IEEE/CVF International Conference on Computer Vision (ICCV)*, pages 8692–8700, 2021. **2, 3, 4, 11, 12**
- [10] Francesco Croce, Maksym Andriushchenko, Vikash Sehwag, Edoardo Debenedetti, Nicolas Flammarion, Mung Chiang, Prateek Mittal, and Matthias Hein. Robustbench: a standardized adversarial robustness benchmark. *ArXiv*, abs/2010.09670, 2021. **2**
- [11] Jia Deng, Wei Dong, Richard Socher, Li-Jia Li, K. Li, and Li Fei-Fei. Imagenet: A large-scale hierarchical image database. In *CVPR*, 2009. **6, 15**
- [12] Alexey Dosovitskiy, Lucas Beyer, Alexander Kolesnikov, Dirk Weissenborn, Xiaohua Zhai, Thomas Unterthiner, Mostafa Dehghani, Matthias Minderer, Georg Heigold, Sylvain Gelly, Jakob Uszkoreit, and Neil Houlsby. An image is worth 16x16 words: Transformers for image recognition at scale. *ArXiv*, abs/2010.11929, 2021. **2, 4, 8**
- [13] Cian Eastwood and Christopher K. I. Williams. A framework for the quantitative evaluation of disentangled representations. In *ICLR*, 2018. **3**
- [14] Mohamed Elhoseiny, Babak Saleh, and Ahmed Elgammal. Write a classifier: Zero-shot learning using purely textual descriptions. In *Proceedings of the IEEE International Conference on Computer Vision*, pages 2584–2591, 2013. **1**
- [15] Ali Farhadi, Ian Endres, Derek Hoiem, and David Forsyth. Describing objects by their attributes. In *2009 IEEE Conference on Computer Vision and Pattern Recognition*, pages 1778–1785, 2009. **1**
- [16] Andrea Frome, Gregory S. Corrado, Jonathon Shlens, Samy Bengio, Jeffrey Dean, Marc’Aurelio Ranzato, and Tomas Mikolov. Devise: A deep visual-semantic embedding model. In *NIPS*, 2013. **2, 3, 11, 12**
- [17] Paul Gavrnikov and Janis Keuper. Cnn filter db: An empirical investigation of trained convolutional filters. *ArXiv*, abs/2203.15331, 2022. **2**
- [18] Ian J. Goodfellow, Jean Pouget-Abadie, Mehdi Mirza, Bing Xu, David Warde-Farley, Sherjil Ozair, Aaron C. Courville, and Yoshua Bengio. Generative adversarial nets. In *NIPS*, 2014. **2, 3**
- [19] Alon Halevy, Peter Norvig, and Fernando Pereira. The unreasonable effectiveness of data. *Intelligent Systems, IEEE*, 24:8–12, 05 2009. **1**
- [20] Zongyan Han, Zhenyong Fu, Shuo Chen, and Jian Yang. Contrastive embedding for generalized zero-shot learning. *2021 IEEE/CVF Conference on Computer Vision and Pattern Recognition (CVPR)*, pages 2371–2381, 2021. **2, 3, 11, 12**
- [21] Kaiming He, Haoqi Fan, Yuxin Wu, Saining Xie, and Ross B. Girshick. Momentum contrast for unsupervised visual representation learning. *2020 IEEE/CVF Conference on Computer Vision and Pattern Recognition (CVPR)*, pages 9726–9735, 2020. **4, 5**
- [22] Kaiming He, X. Zhang, Shaoqing Ren, and Jian Sun. Deep residual learning for image recognition. *2016 IEEE Conference on Computer Vision and Pattern Recognition (CVPR)*, pages 770–778, 2016. **2, 4, 8**
- [23] Chao Jia, Yinfei Yang, Ye Xia, Yi-Ting Chen, Zarana Parekh, Hieu Pham, Quoc V. Le, Yun-Hsuan Sung, Zhen Li, and Tom Duerig. Scaling up visual and vision-language representation learning with noisy text supervision. In *ICML*, 2021. **2**
- [24] Diederik P. Kingma and Max Welling. Auto-encoding variational bayes. *CoRR*, abs/1312.6114, 2014. **2, 3, 4**
- [25] Xia Kong, Zuodong Gao, Xiaofan Li, Ming Hong, Jun Liu, Chengjie Wang, Yuan Xie, and Yanyun Qu. En-compactness: Self-distillation embedding & contrastive generation for generalized zero-shot learning. In *Proceedings of the IEEE/CVF Conference on Computer Vision and Pattern Recognition (CVPR)*, pages 9306–9315, June 2022. **3**
- [26] Alex Krizhevsky, Ilya Sutskever, and Geoffrey E. Hinton. Imagenet classification with deep convolutional neural networks. *Communications of the ACM*, 60:84–90, 2012. **4**
- [27] Gukyeong Kwon and Ghassan Al Regib. A gating model for bias calibration in generalized zero-shot learning. *IEEE Transactions on Image Processing*, pages 1–1, 2022. **2**

- [28] Christoph H Lampert, Hannes Nickisch, and Stefan Harmeling. Attribute-based classification for zero-shot visual object categorization. *IEEE transactions on pattern analysis and machine intelligence*, 36(3):453–465, 2013. [1](#)
- [29] Shichen Liu, Mingsheng Long, Jianmin Wang, and Michael I. Jordan. Generalized zero-shot learning with deep calibration network. In *NeurIPS*, 2018. [2](#)
- [30] Sanath Narayan, Akshita Gupta, Fahad Shahbaz Khan, Cees G. M. Snoek, and Ling Shao. Latent embedding feedback and discriminative features for zero-shot classification. *ArXiv*, abs/2003.07833, 2020. [2](#), [3](#), [5](#), [11](#), [12](#)
- [31] Genevieve Patterson and James Hays. Sun attribute database: Discovering, annotating, and recognizing scene attributes. *2012 IEEE Conference on Computer Vision and Pattern Recognition*, pages 2751–2758, 2012. [3](#), [4](#), [7](#), [13](#), [14](#)
- [32] Farhad Pourpanah, Moloud Abdar, Yuxuan Luo, Xinlei Zhou, Ran Wang, Chee Peng Lim, and Xizhao Wang. A review of generalized zero-shot learning methods. *ArXiv*, abs/2011.08641, 2020. [1](#)
- [33] Alec Radford, Jong Wook Kim, Chris Hallacy, Aditya Ramesh, Gabriel Goh, Sandhini Agarwal, Girish Sastry, Amanda Askell, Pamela Mishkin, Jack Clark, Gretchen Krueger, and Ilya Sutskever. Learning transferable visual models from natural language supervision. In *ICML*, 2021. [2](#), [4](#), [6](#), [11](#)
- [34] Shafin Rahman, Salman Hameed Khan, and Fatih Murat Porikli. A unified approach for conventional zero-shot, generalized zero-shot, and few-shot learning. *IEEE Transactions on Image Processing*, 27:5652–5667, 2018. [2](#)
- [35] Shaoqing Ren, Kaiming He, Ross B. Girshick, and J. Sun. Faster r-cnn: Towards real-time object detection with region proposal networks. *IEEE Transactions on Pattern Analysis and Machine Intelligence*, 39:1137–1149, 2015. [1](#)
- [36] Bernardino Romera-Paredes and Philip H. S. Torr. An embarrassingly simple approach to zero-shot learning. In *ICML*, 2015. [2](#), [3](#), [11](#), [12](#)
- [37] Olga Russakovsky, J. Deng, H. Su, J. Krause, S. Satheesh, S. Ma, Zhiheng Huang, A. Karpathy, A. Khosla, M. Bernstein, A. Berg, and Li Fei-Fei. Imagenet large scale visual recognition challenge. *International Journal of Computer Vision*, 115:211–252, 2015. [1](#)
- [38] Edgar Schönfeld, Sayna Ebrahimi, Samarth Sinha, Trevor Darrell, and Zeynep Akata. Generalized zero- and few-shot learning via aligned variational autoencoders. *2019 IEEE/CVF Conference on Computer Vision and Pattern Recognition (CVPR)*, pages 8239–8247, 2019. [2](#), [3](#), [5](#), [11](#), [12](#)
- [39] Christoph Schuhmann, Richard Vencu, Romain Beaumont, Robert Kaczmarczyk, Clayton Mullis, Aarush Katta, Theo Coombes, Jenia Jitsev, and Aran Komatsuzaki. Laion-400m: Open dataset of clip-filtered 400 million image-text pairs. *ArXiv*, abs/2111.02114, 2021. [6](#), [7](#)
- [40] Yuming Shen, Jie Qin, and Lei Huang. Invertible zero-shot recognition flows. *ArXiv*, abs/2007.04873, 2020. [2](#)
- [41] Amanpreet Singh, Ronghang Hu, Vedanuj Goswami, Guillaume Couairon, Wojciech Galuba, Marcus Rohrbach, and Douwe Kiela. Flava: A foundational language and vision alignment model. *2022 IEEE/CVF Conference on Computer Vision and Pattern Recognition (CVPR)*, pages 15617–15629, 2022. [2](#)
- [42] Hongzu Su, Jingjing Li, Zhi Chen, Lei Zhu, and Ke Lu. Distinguishing unseen from seen for generalized zero-shot learning. In *Proceedings of the IEEE/CVF Conference on Computer Vision and Pattern Recognition (CVPR)*, pages 7885–7894, June 2022. [3](#)
- [43] Chen Sun, Abhinav Shrivastava, Saurabh Singh, and Abhinav Gupta. Revisiting unreasonable effectiveness of data in deep learning era. *CoRR*, abs/1707.02968, 2017. [1](#)
- [44] Flood Sung, Yongxin Yang, Li Zhang, Tao Xiang, Philip H. S. Torr, and Timothy M. Hospedales. Learning to compare: Relation network for few-shot learning. *2018 IEEE/CVF Conference on Computer Vision and Pattern Recognition*, pages 1199–1208, 2018. [4](#)
- [45] Ilya O. Tolstikhin, Neil Houlsby, Alexander Kolesnikov, Lucas Beyer, Xiaohua Zhai, Thomas Unterthiner, Jessica Yung, Daniel Keysers, Jakob Uszkoreit, Mario Lucic, and Alexey Dosovitskiy. Mlp-mixer: An all-mlp architecture for vision. In *NeurIPS*, 2021. [4](#)
- [46] Bin Tong, Chao Wang, Martin Klinkigt, Yoshiyuki Kobayashi, and Yuuichi Nonaka. Hierarchical disentanglement of discriminative latent features for zero-shot learning. *2019 IEEE/CVF Conference on Computer Vision and Pattern Recognition (CVPR)*, pages 11459–11468, 2019. [2](#), [3](#)
- [47] Hugo Touvron, Matthieu Cord, Matthijs Douze, Francisco Massa, Alexandre Sablayrolles, and Hervé J’égou. Training data-efficient image transformers & distillation through attention. In *ICML*, 2021. [4](#)
- [48] Felix Vogel, Nina Shvetsova, Leonid Karlinsky, and Hilde Kuehne. VI-taboo: An analysis of attribute-based zero-shot capabilities of vision-language models. *ArXiv*, abs/2209.06103, 2022. [7](#)
- [49] Catherine Wah, Steve Branson, Peter Welinder, Pietro Perona, and Serge J. Belongie. The caltech-ucsd birds-200-2011 dataset. 2011. [3](#), [4](#), [7](#), [13](#), [14](#), [15](#)
- [50] Yongqin Xian, Christoph H. Lampert, Bernt Schiele, and Zeynep Akata. Zero-shot learning—a comprehensive evaluation of the good, the bad and the ugly. *IEEE Transactions on Pattern Analysis and Machine Intelligence*, 41:2251–2265, 2019. [2](#), [3](#), [4](#), [7](#), [13](#), [14](#)
- [51] Lei Zhang, Peng Wang, Lingqiao Liu, Chunhua Shen, Wei Wei, Yanning Zhang, and Anton van den Hengel. Towards effective deep embedding for zero-shot learning. *IEEE Transactions on Circuits and Systems for Video Technology*, 30:2843–2852, 2020. [2](#)
- [52] Li Zhang, Tao Xiang, and Shaogang Gong. Learning a deep embedding model for zero-shot learning. *2017 IEEE Conference on Computer Vision and Pattern Recognition (CVPR)*, pages 3010–3019, 2017. [2](#)

A. Appendix

In Section B we show implementation details with hyperparameter selections for all GZSL methods, and detail the computing infrastructure we use while conducting all of our experiments. Then we show in fine-tuning information for the multi-modal backbone in Section C. We also show extended results for all of our experiments using all features from different backbones and methods in Section D. Lastly, we discuss about some ethical considerations and the importance of Generalized Zero-Shot Learning in Section E.

B. Implementation Details

We follow the original code and recommended hyperparameters from the existing implementations provided by their corresponding authors for all the GZSL methods in this study. In Table 3 we detail all values for all methods.

B.1. Computing Infrastructure

We performed all the GZSL methods experiments using features extracted from unimodal backbones in 3 servers with 4 NVIDIA TITAN RTX GPUs each. We performed all the GZSL methods experiments using features extracted from multimodal backbones in a single server with 8 NVIDIA A40 GPUs. Feature extraction and fine-tuning were done in a single server with 8 NVIDIA A40 GPUs. All experiments were run on a single GPU.

C. Prompt Engineering for CLIP Fine-Tuning

Prompt for all classes adding class name in the sentence: 'This is a photo of a {}', shown in Table 4.

We also finetune taking into account the attribute **labels** and scores per dataset, shown in Table 5.

D. Full experimental results for our large scale analysis

In this section we show all the results obtained using a large variety of visual backbones from different architecture types. We showcase the performance of all methods, grouped by their corresponding GZSL families and datasets as follows:

- Embedding-based methods
DEVISE [16], ESZSL [36] and ALE [3]:
 - CUB results in Table 6.
 - SUN results in table 7.
 - AWA2 results in table 8.
- Generative-based methods
TF-VAEGAN [30], CADA-VAE [38], CE [20]:
 - CUB results in Table 9.
 - SUN results in table 10.
 - AWA2 results in table 11.
- Semantic disentanglement-based methods
SDGZSL [9], FREE [8]:
 - CUB results in Table 12.
 - SUN results in table 13.
 - AWA2 results in table 14.

Finally, in Table 15, we show full results of generative and disentanglement based methods for the CUB, SUN and AWA2 datasets when using different features extracted from different size and architectures of the visual encoder from all available OpenAI CLIP [33]¹ models.

E. Ethical Considerations

Machine learning models still require collecting large amounts of annotated data. In the case of fine-grained recognition, these annotations often require specialized human knowledge. Zero-shot learning offers a way for bypassing the need to collect extensive amounts of data for training models for new classes of objects. We show that large-scale pre-trained models along with Generalized Zero-Shot Learning methods can obtain results that are competitive with the specialized knowledge from experts on classes that a trained model has never seen. We hope that the key insights and analysis provided in this paper will be useful in expanding and leveraging zero-shot research along with current progress in multi-modal learning. Allowing for the creation of models that do not depend on large amounts of data could be useful for practitioners without access to large scale resources or in domains where data is scarce such as the medical domain.

¹<https://github.com/openai/CLIP>

DEWISE [16]			ESZSL [36]			ALE [3]		
CUB	SUN	AWA2	CUB	SUN	AWA2	CUB	SUN	AWA2
norm = L2 lr = 1.0 mr = 1.0	norm = None lr = 0.01 mr = 3.0	norm = STD lr = 0.001 mr = 150	$\alpha = 3$ $\gamma = 0$	$\alpha = 3$ $\gamma = 2$	$\alpha = 3$ $\gamma = 0$	norm = L2 lr = 0.3	norm = L2 lr = 0.1	norm = L2 lr = 0.01
tfVAEGAN [30]			CADA-VAE [38]			CE [20]		
CUB	SUN	AWA2	CUB	SUN	AWA2	CUB	SUN	AWA2
$\gamma_D = 10$ $\gamma_G = 10$ nepoch = 300 ngh = 4096 ndh = 4096 lr = 0.0001 classifier lr = 0.001 $\lambda = 10$ critic iter = 5 batch size = 64 nz = 312 latent size = 312 syn num = 300 recons weight = 0.01 feed lr = 0.00001 dec lr = 0.0001 feedback loop = 2 manualSeed = 3483	$\gamma_D = 1$ $\gamma_G = 1$ nepoch = 401 ngh = 4096 ndh = 4096 lr = 0.001 classifier lr = 0.0005 $\lambda = 10$ critic iter = 5 batch size = 64 nz = 102 latent size = 102 syn num = 400 recons weight = 0.01 feed lr = 0.0001 dec lr = 0.0001 feedback loop = 2 manualSeed = 4115	$\gamma_D = 10$ $\gamma_G = 10$ nepoch = 300 ngh = 4096 ndh = 4096 lr = 0.00001 classifier lr = 0.001 $\lambda = 10$ critic ite = 5 batch size = 64 nz = 85 latent size = 85 syn num = 1800 recons weight = 0.1 feed lr = 0.0001 dec lr = 0.0001 feedback loop = 2 manualSeed = 9182	lr = 0.00015 cls lr = 0.001 cls loss = L1 β factor = 0.25 cross reconst factor = 2.37 distance factor = 8.13 nepoch = 200 batch size = 100 latent size = 64	lr = 0.00015 cls lr = 0.001 cls loss = L1 β factor = 0.25 cross reconst factor = 2.37 distance factor = 8.13 nepoch = 200 batch size = 100 latent size = 64	syn num = 100 batch size = 2048 attSize = 312 nz = 1024 embedSize = 2048 outzSize = 512 nhF = 2048 ins weight = 0.001 cls weight = 0.001 ins temp = 0.1 cls temp = 0.1 nepoch = 401 manualSeed = 3483	syn num = 100 batch size = 2048 attSize = 312 nz = 1024 embedSize = 2048 outzSize = 512 nhF = 2048 ins weight = 0.001 cls weight = 0.001 ins temp = 0.1 cls temp = 0.1 nepoch = 401 manualSeed = 4115	syn num = 1800 batch size = 4096 attSize = 312 nz = 1024 embedSize = 2048 outzSize = 512 nhF = 2048 ins weight = 0.001 cls weight = 0.001 ins temp = 10.0 cls temp = 1.0 nepoch = 131 manualSeed = 9182	
SDGZSL [9]			FREE [8]					
CUB	SUN	AWA2	CUB	SUN	AWA2			
$\gamma = 5$ $\beta = 0.003$ dis = 0.3 nSample = 1000 lr = 0.0001 classifier lr = 0.002 nepoch = 600 kl warmup = 0.001 tc warmup = 0.0001 weight decay = 1e-8 vae enc drop = 0.1 vae dec drop = 0.1 dis step = 3 ae drop = 0.0	$\gamma = 30$ $\beta = 0.3$ dis = 0.5 nSample = 400 lr = 0.0003 kl warmup = 0.001 tc warmup = 0.0003 vae dec drop = 0.2 dis step = 3 ae drop = 0.4	$\gamma = 0.5$ $\beta = 1$ dis = 0.3 nSample = 5000 lr = 0.00003 classifier lr = 0.003 kl warmup = 0.01 tc warmup = 0.001 vae dec drop = 0.5 vae enc drop = 0.4 dis step = 2 ae drop = 0.2 gen nepoch = 220 evl start = 40000 evl interval = 400 manualSeed = 6152	nepoch = 201 ngh = 4096 lr = 0.0001 classifier lr = 0.001 $\lambda = 10$ critic iter = 1 feed lr = 0.00001 dec lr = 0.0001 loop = 2 batch size = 64 nz = 312 latent size = 312 syn num = 700 center margin = 200 center weight = 0.5 recons weight = 0.001 incenter weight = 0.8 manualSeed = 3483	nepoch = 601 ngh = 4096 loop = 2 feed lr = 0.0001 ndh = 4096 $\lambda = 10$ critic iter = 1 batch size = 512 nz = 102 latent size = 102 lr = 0.0002 classifier lr = 0.0005 syn num = 300 center margin = 120 incenter weight = 0.8 center weight = 0.5 recons weight = 0.1 manualSeed = 4115	nepoch = 401 ngh = 4096 $\lambda = 10$ critic iter = 1 feed lr = 0.0001 dec lr = 0.0001 loop = 2 batch size = 64 nz = 85 latent size = 85 lr = 0.00001 classifier lr = 0.001 syn num = 4600 center margin = 50 center weight = 0.5 recons weight = 0.001 incenter weight = 0.5 manualSeed = 9182			

Table 3. Hyper-parameter selection details for all methods.

CUB [49]

Black footed Albatross	Laysan Albatross	Sooty Albatross	Groove billed Ani	Crested Auklet
Least Auklet	Parakeet Auklet	Rhinoceros Auklet	Brewer Blackbird	Red winged Blackbird
Rusty Blackbird	Yellow headed Blackbird	Bobolink	Indigo Bunting	Lazuli Bunting
Painted Bunting	Cardinal	Spotted Catbird	Gray Catbird	Yellow breasted Chat
Eastern Towhee	Chuck will Widow	Brandt Cormorant	Red faced Cormorant	Pelagic Cormorant
Bronzed Cowbird	Shiny Cowbird	Brown Creeper	American Crow	Fish Crow
Black billed Cuckoo	Mangrove Cuckoo	Yellow billed Cuckoo	Gray crowned Rosy Finch	Purple Finch
Northern Flicker	Acadian Flycatcher	Great Crested Flycatcher	Least Flycatcher	Olive sided Flycatcher
Scissor tailed Flycatcher	Vermilion Flycatcher	Yellow bellied Flycatcher	Frigatebird	Northern Fulmar
Gadwall	American Goldfinch	European Goldfinch	Boat tailed Grackle	Eared Grebe
Horned Grebe	Pied billed Grebe	Western Grebe	Blue Grosbeak	Evening Grosbeak
Pine Grosbeak	Rose breasted Grosbeak	Pigeon Guillemot	California Gull	Glaucous winged Gull
Heermann Gull	Herring Gull	Ivory Gull	Ring billed Gull	Slaty backed Gull
Western Gull	Anna Hummingbird	Ruby throated Hummingbird	Rufous Hummingbird	Green Violetear
Long tailed Jaeger	Pomarine Jaeger	Blue Jay	Florida Jay	Green Jay
Dark eyed Junco	Tropical Kingbird	Gray Kingbird	Belted Kingfisher	Green Kingfisher
Pied Kingfisher	Ringed Kingfisher	White breasted Kingfisher	Red legged Kittiwake	Horned Lark
Pacific Loon	Mallard	Western Meadowlark	Hooded Merganser	Red breasted Merganser
Mockingbird	Nighthawk	Clark Nutcracker	White breasted Nuthatch	Baltimore Oriole
Hooded Oriole	Orchard Oriole	Scott Oriole	Ovenbird	Brown Pelican
White Pelican	Western Wood Pewee	Sayornis	American Pipit	Whip poor Will
Horned Puffin	Common Raven	White necked Raven	American Redstart	Geococcyx
Loggerhead Shrike	Great Grey Shrike	Baird Sparrow	Black throated Sparrow	Brewer Sparrow
Chipping Sparrow	Clay colored Sparrow	House Sparrow	Field Sparrow	Fox Sparrow
Grasshopper Sparrow	Harris Sparrow	Henslow Sparrow	Le Conte Sparrow	Lincoln Sparrow
Nelson Sharp tailed Sparrow	Savannah Sparrow	Seaside Sparrow	Song Sparrow	Tree Sparrow
Vesper Sparrow	White crowned Sparrow	White throated Sparrow	Cape Glossy Starling	Bank Swallow
Barn Swallow	Cliff Swallow	Tree Swallow	Scarlet Tanager	Summer Tanager
Artic Tern	Black Tern	Caspian Tern	Common Tern	...

SUN [31]

abbey	access road	airfield	airlock	airplane cabin
airport airport	airport entrance	airport terminal	airport ticket counter	alcove
alley	amphitheater	amusement arcade	amusement park	anechoic chamber
apartment building outdoor	apse indoor	apse outdoor	aquarium	aquatic theater
aqueduct	arch	archaeological excavation	archive	arena basketball
arena hockey	arena performance	armory	arrival gate outdoor	art gallery
art school	art studio	artists loft	assembly line	athletic field outdoor
atrium home	atrium public	attic	auditorium	auto factory
auto mechanics indoor	auto racing paddock	auto showroom	backstage	badlands
badminton court indoor	badminton court outdoor	baggage claim	bakery kitchen	bakery shop
balcony exterior	balcony interior	ball pit	ballroom	bamboo forest
bank indoor	bank outdoor	bank vault	banquet hall	baptistry indoor
baptistry outdoor	bar	barn	barndoor	baseball field
basement	basilica	basketball court indoor	basketball court outdoor	bathroom
batters box	batting cage indoor	batting cage outdoor	bayou	bazaar indoor
bazaar outdoor	beach	beach house	beauty salon	bedchamber
bedroom	beer garden	beer hall	bell foundry	berth
betting shop	bicycle racks	bindery	biology laboratory	bistro indoor
bistro outdoor	bleachers outdoor	boardwalk	boat deck	boathouse
bog	bookstore	booth indoor	botanical garden	bow window indoor
bow window outdoor	bowling alley	boxing ring	brewery indoor	brewery outdoor
brickyard outdoor	bridge	building complex	building facade	bullpen
bullring	burial chamber	bus depot outdoor	bus interior	bus shelter
bus station outdoor	butchers shop	butte	cabana	cabin outdoor
cafeteria	call center	campsite	campus	canal natural
canal urban	candy store	canteen	canyon	car interior backseat
car interior frontseat	caravansary	cardroom	cargo deck airplane	carport freestanding
carport outdoor	carrousel	casino indoor	casino outdoor	castle
catacomb	cathedral indoor	cathedral outdoor	catwalk	cavern indoor
cemetery	chalet	chaparral	chapel	checkout counter
cheese factory	chemical plant	chemistry lab	chicken coop indoor	...

AWA2 [50]

antelope	grizzly bear	killer whale	beaver	dalmatian
persian cat	horse	german shepherd	blue whale	siamese cat
skunk	mole	tiger	hippopotamus	leopard
moose	spider monkey	humpback whale	elephant	gorilla
ox	fox	sheep	seal	chimpanzee
hamster	squirrel	rhinoceros	rabbit	bat
giraffe	wolf	chihuahua	rat	weasel
otter	buffalo	zebra	giant panda	deer
bobcat	pig	lion	mouse	polar bear
collie	walrus	raccoon	cow	dolphin

Table 4. Some class names per dataset.

Prompt: 'Image of a bird with {}'				
curved (up or down) bill shape	dagger bill shape	hooked bill shape	needle bill shape	hooked seabird bill shape
spatulate bill shape	all-purpose bill shape	cone bill shape	specialized bill shape	blue wings
brown wings	iridescent wings	purple wings	rufous wings	grey wings
yellow wings	olive wings	green wings	pink wings	orange wings
black wings	white wings	red wings	buff wings	blue upperparts
brown upperparts	iridescent upperparts	purple upperparts	rufous upperparts	grey upperparts
yellow upperparts	olive upperparts	green upperparts	pink upperparts	orange upperparts
black upperparts	white upperparts	red upperparts	buff upperparts	blue underparts
brown underparts	iridescent underparts	purple underparts	rufous underparts	grey underparts
yellow underparts	olive underparts	green underparts	pink underparts	orange underparts
black underparts	white underparts	red underparts	buff underparts	solid breast pattern
spotted breast pattern	striped breast pattern	multi-ed breast pattern	blue back	brown back
iridescent back	purple back	rufous back	grey back	yellow back
olive back	green back	pink back	orange back	black back
white back	red back	buff back	forked tail tail shape	rounded tail tail shape
notched tail tail shape	fan-shaped tail tail shape	pointed tail tail shape	squared tail tail shape	blue upper tail
brown upper tail	iridescent upper tail	purple upper tail	rufous upper tail	orange upper tail
yellow upper tail	olive upper tail	green upper tail	pink upper tail	spotted head pattern
black upper tail	white upper tail	red upper tail	buff upper tail	eyebrow head pattern
malar head pattern	crested head pattern	masked head pattern	unique pattern head pattern	capped head pattern
eyering head pattern	plain head pattern	eyeline head pattern	striped head pattern	iridescent breast
blue breast	brown breast	olive breast	purple breast	green breast
grey breast	black breast	white breast	red breast	pink breast
orange breast	yellow breast	black breast	buff breast	buff breast
blue throat	brown throat	iridescent throat	purple throat	rufous throat
grey throat	yellow throat	olive throat	green throat	pink throat
orange throat	black throat	white throat	red throat	buff throat
blue eye	brown eye	purple eye	rufous eye	grey eye
yellow eye	olive eye	green eye	pink eye	orange eye
black eye	white eye	red eye	buff eye	broad-wings wing shape
tapered-wings wing shape	long-wings wing shape	blue forehead	brown forehead	iridescent forehead
purple forehead	rufous forehead	grey forehead	yellow forehead	olive forehead
green forehead	pink forehead	orange forehead	black forehead	white forehead
red forehead	buff forehead	blue under tail	brown under tail	iridescent under tail
purple under tail	rufous under tail	grey under tail	yellow under tail	olive under tail
green under tail	pink under tail	orange under tail	black under tail	white under tail
red under tail	buff under tail	blue nape	brown nape	iridescent nape
purple nape	rufous nape	grey nape	yellow nape	olive nape
green nape	pink nape	orange nape	black nape	white nape
red nape	buff nape	blue belly	brown belly	iridescent belly
purple belly	rufous belly	grey belly	yellow belly	olive belly
green belly	pink belly	orange belly	black belly	white belly
red belly	buff belly	rounded-wings wing shape	pointed-wings wing shape	broad-wings wing shape
iridescent primary	purple primary	rufous primary	grey primary	yellow primary
olive primary	green primary	pink primary	orange primary	black primary
white primary	red primary	buff primary	blue leg	brown leg
iridescent leg	purple leg	rufous leg	grey leg	yellow leg
olive leg	green leg	pink leg	orange leg	black leg
white leg	red leg	buff leg	blue bill	...

SUN [31]

Prompt: 'Image of a place for {}'				
Prompt: 'Image of a place with {}'				
sailing or boating	driving	biking	transporting things or people	sunbathing
vacationing or touring	hiking	climbing	camping	reading
studying or learning	teaching or training	research	diving	swimming
bathing	eating	cleaning	socializing	congregating
waiting in line or queuing	competing	sports	exercise	playing
gaming	spectating or being in an audience	farming	constructing or building	shopping
medical activity	working	using tools	digging	conducting business
praying	fencing	railing	wire	railroad
trees	grass	vegetation	shrubbery	foliage
leaves	flowers	asphalt	pavement	shingles
carpet	brick	tiles	concrete	metal
paper	wood (not part of a tree)	vinyl or linoleum	rubber or plastic	cloth
sand	rock or stone	dirt or soil	marble	glass
waves or surf	ocean	running water	still water	ice
snow	clouds	smoke	fire	...

AWA2 [50]

Prompt: 'Image of an animal with {}'				
Prompt: 'Image of an animal that {}'				
Prompt: 'Image of an animal that lives in the {}'				
Prompt: 'Image of a {} animal'				
black	white	blue	brown	gray
orange	red	yellow	patches	spots
stripes	furry	hairless	toughskin	big
small	bulbous	lean	flippers	hands
hooves	pads	paws	longleg	longneck
tail	chewteeth	meatteeth	buckteeth	strainteeth
horns	claws	tusks	smelly	flies
hops	swims	tunnels	walks	fast
slow	strong	weak	muscle	bipedal
quadrupedal	active	inactive	nocturnal	hibernate
agility	fish	meat	plankton	vegetation
insects	forager	grazer	hunter	scavenger
skimmer	stalker	newworld	oldworld	arctic
coastal	desert	bush	plains	forest
fields	jungle	mountains	ocean	ground
water	tree	cave	fierce	timid
smart	group	solitary	nestspot	domestic

Table 5. Prompt and some class attributes labels per dataset.

Embedding Based GZSL Methods											
CUB [49] Dataset											
Dataset	Arch Type	Backbone	DEWISE			ESZSL			ALE		
			Seen	Novel	Harm.	Seen	Novel	Harm.	Seen	Novel	Harm.
I-1k	CNN	RN101	61.96	23.41	33.98	56.53	14.70	23.34	62.74	26.07	36.83
		RN101+FT	83.42	28.32	42.28	81.45	16.14	26.94	83.04	30.36	44.46
		RN50	41.32	17.31	24.39	41.83	13.78	20.73	45.96	24.70	32.13
		RN152	45.73	19.01	26.86	46.39	15.49	23.23	52.69	24.84	33.76
		GoogleNet	35.57	15.10	21.20	30.79	9.70	14.75	36.86	17.67	23.89
		VGG16	44.11	14.93	22.30	46.74	7.29	12.61	45.81	18.26	26.11
		Alexnet	33.57	13.04	18.78	33.65	5.62	9.64	33.15	14.82	20.48
		Shufflenet	47.24	20.05	28.15	22.16	12.13	15.67	48.15	22.18	30.37
		Inceptionv3	58.09	21.81	31.71	48.30	12.91	20.38	53.11	21.52	30.63
		Inceptionv3 _{adv}	54.84	20.86	30.22	47.70	11.09	18.00	59.37	20.24	30.18
		RN50-MOCO [†]	31.26	11.39	16.70	7.69	3.87	5.15	32.73	15.77	21.28
		RN50-DINO [†]	63.20	25.84	36.68	41.65	14.64	21.67	60.69	25.79	36.19
	MLP	MLP-Mixer	19.17	7.76	11.05	20.50	5.53	8.71	19.82	8.11	11.51
	ViT	ViT _{large}	71.85	23.88	35.85	83.64	12.26	21.39	72.20	23.44	35.39
		DeiT _{base}	70.45	25.86	37.83	60.88	16.81	26.35	73.88	30.88	43.55
		ViTB16-DINO [†]	75.50	32.20	45.15	70.89	29.06	41.23	77.21	36.83	49.87
	MLP	MLP-Mixer _{L16}	38.46	12.02	18.32	34.62	5.82	9.97	41.66	10.68	17.00
I-21k	ViT	ViT _{base}	84.52	26.75	40.64	81.33	19.57	31.55	83.39	29.59	43.68
		ViT _{large}	85.24	25.61	39.38	82.47	17.53	28.92	83.09	22.08	34.89
		ViT _{huge}	82.78	31.31	45.44	61.88	18.77	28.80	84.00	36.05	50.45

Table 6. Results of Embedding Based Methods for the CUB [49] dataset using different features extracted from a diverse set of architecture types pretrained on ImageNet-1k (I-1k) and ImageNet-21k (I-21k) [11]. These backbones were trained via: supervised and self-supervised ([†]) learning. The bold numbers correspond to the highest scores per column, and the shaded rows correspond to the most performant image feature per method. +FT indicates the features were fine-tuned with the seen classes from the training set. The ViT_{huge} features pretrained on ImageNet-21k are the best for all the methods using ALE.

Embedding Based GZSL Methods											
SUN Dataset											
Dataset	Arch	Backbone	DEVISE			ESZSL			ALE		
			Seen	Novel	Harm.	Seen	Novel	Harm.	Seen	Novel	Harm.
I-1k	CNN	RN101	32.75	18.54	23.68	28.41	13.75	18.53	37.13	23.68	28.92
		RN101+FT	34.03	19.93	25.14	33.18	13.82	19.51	37.95	22.43	28.19
		RN50	29.84	17.43	22.01	25.08	14.38	18.27	33.91	23.54	27.79
		RN152	30.39	17.29	22.04	26.63	15.90	19.91	35.70	23.40	28.27
		GoogleNet	18.02	10.83	13.53	17.52	9.31	12.15	24.88	15.76	19.30
		VGG16	28.91	13.06	17.99	25.85	9.93	14.35	31.78	20.21	24.71
		Alexnet	19.61	9.31	12.62	19.03	6.88	10.10	23.60	13.82	17.43
		Shufflenet	0.23	0.00	0.00	0.74	1.74	1.03	29.53	17.78	22.20
		Inceptionv3	31.01	14.03	19.32	25.08	11.25	15.53	32.29	18.47	23.50
		Inceptionv3 _{adv}	27.91	15.00	19.51	24.69	12.08	16.23	33.88	21.39	26.22
		RN50-MOCO [†]	2.25	0.00	0.00	3.14	3.33	3.23	34.92	23.33	27.98
		RN50-DINO [†]	32.56	19.03	24.02	22.48	14.65	17.74	41.59	27.57	33.16
MLP	MLP-Mixer	6.32	3.33	4.36	6.40	2.36	3.45	8.29	3.96	5.36	
ViT	ViT _{large}	52.33	24.51	33.39	44.84	18.82	26.51	59.77	34.10	43.42	
	DeiT _{base}	37.17	17.22	23.54	28.49	12.57	17.44	38.37	21.53	27.58	
	ViTB16-DINO [†]	35.19	20.97	26.28	32.48	16.11	21.54	40.89	28.40	33.52	
MLP	MLP-Mixer _{L16}	24.57	11.18	15.37	20.74	9.24	12.78	29.03	13.61	18.53	
I-21k	ViT	ViT _{base}	45.19	25.07	32.25	40.43	19.51	26.32	52.87	31.81	39.72
		ViT _{large}	49.15	25.56	33.63	43.29	19.86	27.23	55.23	33.26	41.52
		ViT _{huge}	38.22	19.24	25.59	31.71	18.13	23.06	51.55	30.07	37.98

Table 7. Results of Embedding Based Methods for the SUN dataset using different features extracted from a diverse set of architecture types pretrained on ImageNet-1k (I-1k) and ImageNet-21k (I-21k). These backbones were trained via: supervised and self-supervised ([†]) learning. The bold numbers correspond to the highest scores per column, and the shaded rows correspond to the most performant image feature per method. +FT indicates the features were fine-tuned with the seen classes from the training set. Surprisingly, Shufflenet and RN50-MOCO features seem to be not suited for this dataset, and using ViT_{large} pretrained on ImageNet-1k features with ALE beat all methods, including its counterpart pretrained on ImageNet-21k by a reasonable margin (1.9%). Moreover, using the ViT_{large} pretrained on ImageNet-21k features beats all other methods when using DEVISE and ESZSL.

Embedding Based GZSL Methods											
AWA2 Dataset											
Dataset Pret. on	Arch Type	Backbone	DEVISE			ESZSL			ALE		
			<i>Seen</i>	<i>Novel</i>	<i>Harm.</i>	<i>Seen</i>	<i>Novel</i>	<i>Harm.</i>	<i>Seen</i>	<i>Novel</i>	<i>Harm.</i>
I-1k	CNN	RN101	71.78	17.30	27.88	88.84	4.04	7.72	77.59	12.15	21.01
		RN101+FT	87.34	18.83	30.99	93.07	6.12	11.49	92.64	8.25	15.16
		RN50	86.02	19.49	31.78	89.05	4.75	9.02	84.37	10.48	18.65
		RN152	88.30	21.18	34.17	91.31	5.94	11.15	85.46	12.91	22.43
		GoogleNet	68.56	17.40	27.76	80.11	4.26	8.10	82.82	5.13	9.66
		VGG16	78.85	16.21	26.89	90.06	3.11	6.00	77.34	11.52	20.06
		Alexnet	72.91	12.17	20.86	79.09	2.77	5.36	79.17	6.11	11.34
		Shufflenet	74.74	20.04	31.61	51.66	3.69	6.89	80.75	8.84	15.93
		Inceptionv3	74.54	8.08	14.58	91.49	4.43	8.46	78.24	10.32	18.23
		Inceptionv3 _{adv}	89.33	12.14	21.38	91.69	3.53	6.79	82.21	8.06	14.69
	RN50-MOCO [†]	78.23	11.07	19.39	57.62	3.73	7.01	81.51	4.60	8.71	
	RN50-DINO [†]	78.97	18.11	29.46	81.25	8.08	14.71	82.78	7.62	13.96	
	MLP	MLP-Mixer	21.06	10.87	14.34	38.51	2.67	4.99	94.29	12.78	22.52
	ViT	ViT _{large}	83.78	18.00	29.63	97.07	18.62	31.25	92.28	13.75	23.93
	DeiT _{base}	91.41	9.51	17.22	94.08	2.33	4.54	87.37	14.67	25.12	
	ViTB16-DINO [†]	71.83	19.41	30.56	92.34	5.08	9.63	79.73	6.55	12.10	
I-21k	MLP	MLP-Mixer _{L16}	82.92	10.37	18.43	85.48	1.47	2.90	86.24	1.88	3.69
	ViT	ViT _{base}	82.35	14.05	24.00	96.18	7.77	14.38	95.62	11.07	19.85
		ViT _{large}	86.49	19.53	31.87	96.47	10.43	18.83	95.03	12.76	22.49
		ViT _{huge}	80.00	12.37	21.43	89.57	2.55	4.95	81.40	6.72	12.41

Table 8. Results of Embedding Based Methods for the AWA2 dataset using different features extracted from a diverse set of architecture types pretrained on ImageNet-1k (I-1k) and ImageNet-21k (I-21k). These backbones were trained via: supervised and self-supervised ([†]) learning. The bold numbers correspond to the highest scores per column, and the shaded rows correspond to the most performant image feature per method. +FT indicates the features were fine-tuned with the seen classes from the training set. Surprisingly, the most performant visual features are extracted from a RN152 pretrained on ImageNet-1k, using the DEVISE method.

Generative Based GZSL Methods CUB Dataset												
Dataset Pref. on	Arch Type	Backbone	tfVAEGAN			CADA-VAE			CE			
			Seen	Novel	Harm.	Seen	Novel	Harm.	Seen	Novel	Harm.	
I-1k	CNN	RN101	57.08	42.88	48.97	58.27	49.71	53.65	60.09	49.05	54.01	
		RN101+FT	72.44	53.66	61.65	76.45	57.53	65.65	76.71	48.81	59.66	
		RN50	49.29	42.35	45.55	45.88	38.95	42.13	42.79	35.46	38.78	
		RN152	50.23	44.48	47.18	47.58	41.64	44.41	45.77	35.52	40.00	
		GoogleNet	38.54	33.34	35.76	33.84	30.20	31.92	33.72	26.05	29.39	
		VGG16	36.67	38.46	37.54	37.12	35.38	36.23	35.00	37.84	36.36	
		Alexnet	21.48	32.52	25.87	22.36	24.31	23.29	23.73	28.62	25.95	
		Shufflenet	51.62	43.83	47.41	43.14	38.56	40.72	48.95	37.69	42.59	
		Inceptionv3	54.01	50.41	52.15	50.32	39.87	44.49	54.80	38.45	45.19	
		Inceptionv3 _{adv}	62.81	41.34	49.86	50.28	37.90	43.22	54.83	35.41	43.03	
I-21k	MLP	RN50-MOCO [†]	41.88	29.13	34.36	27.40	22.39	24.64	34.01	24.09	28.21	
		RN50-DINO [†]	64.11	53.84	58.53	55.05	47.59	51.05	62.45	45.13	52.39	
		MLP-Mixer	18.64	15.87	17.15	11.74	18.45	14.35	10.99	10.94	10.97	
		ViT	ViT _{large}	80.34	54.34	64.83	61.23	53.31	56.99	70.22	43.07	53.39
			DeiT _{base}	73.29	49.44	59.05	60.39	50.05	54.74	55.68	38.68	45.65
			ViTB16-DINO [†]	76.82	57.94	66.06	71.95	55.37	62.58	61.29	45.47	52.21
		MLP-Mixer _{L16}	30.91	28.77	29.80	28.68	25.19	26.82	17.46	20.76	18.96	
		ViT	ViT _{base}	74.16	71.13	72.61	74.46	60.77	66.93	61.01	51.25	55.71
			ViT _{large}	76.95	61.56	68.40	72.54	58.94	65.04	67.16	46.94	55.26
			ViT _{huge}	75.15	62.76	68.40	70.53	60.50	65.13	49.37	43.76	46.40
ViT _{huge} +FT	78.32		76.26	77.27	77.99	74.46	76.18	70.87	44.66	54.79		

Table 9. Results of Generative Based Methods for the CUB dataset using different features extracted from a diverse set of architecture types pretrained on ImageNet-1k (I-1k) and ImageNet-21k (I-21k). These backbones were trained via: supervised and self-supervised ([†]) learning. The bold numbers correspond to the highest scores per column, and the shaded rows correspond to the most performant image feature per method. +FT indicates the features were fine-tuned with the seen classes from the training set. The most performant visual features are extracted from a ViT_{huge} pretrained on ImageNet-21k and fine-tuned with the seen classes, using the tfVAEGAN method.

Generative Based GZSL Methods SUN Dataset											
Dataset Pret. on	Arch Type	Backbone	tfVAEGAN			CADA-VAE			CE		
			<i>Seen</i>	<i>Novel</i>	<i>Harm.</i>	<i>Seen</i>	<i>Novel</i>	<i>Harm.</i>	<i>Seen</i>	<i>Novel</i>	<i>Harm.</i>
I-1k	CNN	RN101	38.95	45.62	42.03	34.15	48.96	40.23	51.24	55.83	53.44
		RN101+FT	35.08	38.06	36.51	39.84	51.60	44.97	29.07	38.75	33.22
		RN50	34.61	45.07	39.15	34.07	41.53	37.43	23.95	42.36	30.60
		RN152	35.35	45.97	39.97	37.05	40.00	38.47	26.20	43.33	32.66
		GoogleNet	27.17	38.26	31.78	24.96	36.32	29.59	20.43	38.96	26.80
		VGG16	25.04	28.61	26.71	31.32	37.85	34.27	24.11	36.81	29.13
		Alexnet	25.27	34.72	29.25	16.51	23.06	19.24	13.84	30.90	19.12
		Shufflenet	31.59	42.71	36.32	30.62	37.64	33.77	24.92	37.50	29.94
		Inceptionv3	30.00	32.15	31.04	32.64	38.26	35.23	26.09	37.43	30.74
		Inceptionv3 _{adv}	33.37	45.42	38.47	32.02	40.83	35.89	27.09	39.44	32.12
	RN50-MOCO [†]	37.44	42.99	40.02	35.08	38.13	36.54	30.62	44.24	36.19	
	RN50-DINO [†]	42.60	46.67	44.54	41.16	46.39	43.62	29.38	55.56	38.43	
	MLP	MLP-Mixer	24.96	32.22	28.13	6.82	12.78	8.89	8.64	8.33	8.49
	I-21k	ViT	ViT _{large}	55.12	64.93	59.62	52.64	61.32	56.65	50.70	52.78
DeiT _{base}			34.34	44.72	38.85	37.44	44.51	40.67	36.36	37.57	36.95
ViTB16-DINO [†]			42.64	52.71	47.14	42.52	51.18	46.45	40.39	45.56	42.82
MLP		MLP-Mixer _{L16}	24.22	43.03	28.30	24.77	29.65	26.99	23.84	20.00	21.75
ViT		ViT _{base}	54.19	58.75	56.38	52.02	60.14	55.78	51.53	50.74	51.13
		ViT _{large}	57.13	61.32	59.15	52.83	60.69	56.49	50.12	50.69	50.40
		ViT _{huge}	43.37	53.61	47.95	47.64	51.18	49.34	49.79	16.05	24.27
		ViT _{huge} +FT	44.26	54.24	48.75	44.99	55.35	49.64	6.86	53.61	12.16

Table 10. Results of Generative Based Methods for the SUN dataset using different features extracted from a diverse set of architecture types pretrained on ImageNet-1k (I-1k) and ImageNet-21k (I-21k). These backbones were trained via: supervised and self-supervised ([†]) learning. The bold numbers correspond to the highest scores per column, and the shaded rows correspond to the most performant image feature per method. +FT indicates the features were fine-tuned with the seen classes from the training set. Surprisingly, the CE method does not seem to get any significant advantage from any of the ViT features, and overall, the most performant visual features are extracted from a ViT_{large} pretrained on ImageNet-1k using the tfVAEGAN method.

Generative Based GZSL Methods AWA2 Dataset											
Dataset Pret. on	Arch Type	Backbone	tfVAEGAN			CADA-VAE			CE		
			<i>Seen</i>	<i>Novel</i>	<i>Harm.</i>	<i>Seen</i>	<i>Novel</i>	<i>Harm.</i>	<i>Seen</i>	<i>Novel</i>	<i>Harm.</i>
I-1k	CNN	RN101	75.48	59.56	66.58	75.95	54.76	63.87	69.26	56.03	61.95
		RN101+FT	84.81	58.44	69.20	77.74	59.95	69.14	83.43	47.66	60.66
		RN50	79.91	55.83	65.73	74.56	59.48	67.80	71.72	46.65	56.53
		RN152	84.48	60.01	70.17	88.88	57.69	70.48	76.74	40.25	52.8
		GoogleNet	69.08	55.17	61.35	71.51	53.22	62.22	73.36	47.63	57.76
		VGG16	78.95	52.54	63.09	74.17	58.92	67.26	62.37	46.85	53.51
		Alexnet	64.31	41.11	50.16	61.98	40.80	49.60	57.13	39.39	46.63
		Shufflenet	69.53	55.38	61.66	68.07	54.09	61.84	71.87	50.11	59.05
		Inceptionv3	84.00	58.45	68.94	78.97	61.77	70.86	74.69	52.09	61.38
		Inceptionv3 _{adv}	85.48	59.21	69.96	82.15	53.43	65.23	66.96	53.73	59.62
		RN50-MOCO [†]	68.51	51.75	58.96	65.52	55.53	62.02	64.77	40.92	50.15
	RN50-DINO [†]	74.58	60.00	66.50	73.36	55.23	64.30	74.22	45.46	56.38	
	MLP	MLP-Mixer	28.14	25.27	26.63	14.01	41.56	27.90	22.93	20.68	21.75
	ViT	ViT _{large}	90.14	68.28	77.70	85.55	70.62	79.25	81.37	69.14	74.75
		DeiT _{base}	84.63	51.89	64.33	77.83	59.04	68.50	79.35	50.62	61.81
		ViTB16-DINO [†]	77.64	57.77	66.24	75.69	63.90	71.25	81.66	54.65	65.48
I-21k	MLP	MLP-Mixer _{L16}	72.63	42.47	53.60	70.15	51.01	60.12	61.51	39.01	47.74
	ViT	ViT _{base}	54.19	58.75	56.38	84.48	67.42	76.67	77.80	49.54	60.53
		ViT _{large}	91.05	63.58	74.87	88.69	70.75	80.40	78.32	59.21	67.44
		ViT _{huge}	88.85	60.79	72.19	85.68	60.95	72.25	75.57	53.24	62.47
		ViT _{huge} +FT	68.23	61.63	64.76	80.69	60.76	69.32	75.23	60.10	66.82

Table 11. Results of Generative Based Methods for the AWA2 dataset using different features extracted from a diverse set of architecture types pretrained on ImageNet-1k (I-1k) and ImageNet-21k (I-21k). These backbones were trained via: supervised and self-supervised ([†]) learning. The bold numbers correspond to the highest scores per column, and the shaded rows correspond to the most performant image feature per method. +FT indicates the features were fine-tuned with the seen classes from the training set. The most performant visual features are extracted from a ViT_{huge} pretrained on ImageNet-21k and fine-tuned with the seen classes, using the CADA-VAE method. More interestingly, the features from a ViT_{large} pretrained on ImageNet-1k seem competitive with the features from a ViT_{large} pretrained on ImageNet-21k for the CE and tfVAEGAN methods respectively.

Disentanglement Based GZSL Methods								
CUB Dataset								
Dataset Pret. on	Arch Type	Backbone	SDGZSL			FREE		
			<i>Seen</i>	<i>Novel</i>	<i>Harm.</i>	<i>Seen</i>	<i>Novel</i>	<i>Harm.</i>
I-1k	CNN	RN101	56.41	51.89	54.06	58.30	55.10	56.70
		RN101+FT	75.00	64.26	69.21	75.30	56.00	64.20
		RN50	48.48	37.53	42.31	48.40	41.10	44.45
		RN152	48.22	43.37	45.67	50.70	43.90	47.10
		GoogleNet	32.72	32.88	32.80	33.78	34.34	34.06
		VGG16	37.20	34.41	35.75	30.02	40.14	34.35
		Alexnet	27.12	24.98	26.01	15.47	34.16	21.30
		Shufflenet	47.66	38.90	42.84	47.65	43.64	45.56
		Inceptionv3	56.70	46.39	51.03	61.88	44.60	51.83
		Inceptionv3 _{adv}	51.38	46.86	49.01	60.82	42.02	49.70
		RN50-MOCO [†]	36.67	30.22	33.14	42.53	29.38	34.75
		RN50-DINO [†]	59.27	51.68	55.22	66.62	53.08	59.08
	MLP	MLP-Mixer	17.66	16.74	17.19	17.59	14.43	15.85
	ViT	ViT _{large}	74.17	63.17	68.23	69.53	56.38	62.27
		DeiT _{base}	62.91	54.40	58.35	61.80	43.80	51.27
		ViTB16-DINO [†]	68.72	64.25	66.41	73.70	53.46	61.97
	MLP	MLP-Mixer _{L16}	33.77	26.13	29.46	31.58	23.61	27.02
I-21k	ViT	ViT _{base}	78.01	70.10	73.84	67.50	66.15	66.82
		ViT _{large}	79.55	64.37	71.16	73.07	52.91	61.37
		ViT _{huge}	75.05	70.58	72.75	66.17	67.57	66.87
		ViT _{huge} +FT	79.68	73.27	76.34	80.57	69.71	74.75

Table 12. Results of Disentanglement Based Methods for the CUB dataset using different features extracted from a diverse set of architecture types pretrained on ImageNet-1k (I-1k) and ImageNet-21k (I-21k). These backbones were trained via: supervised and self-supervised ([†]) learning. The bold numbers correspond to the highest scores per column, and the shaded rows correspond to the most performant image feature per method. +FT indicates the features were fine-tuned with the seen classes from the training set. The most performant visual features are extracted from a ViT_{huge} pretrained on ImageNet-21k and fine-tuned with the seen classes, using the SDGZSL method.

Disentanglement Based GZSL Methods								
SUN Dataset								
Dataset Pref. on	Arch Type	Backbone	SDGZSL			FREE		
			<i>Seen</i>	<i>Novel</i>	<i>Harm.</i>	<i>Seen</i>	<i>Novel</i>	<i>Harm.</i>
I-1k	CNN	RN101	36.67	44.44	40.18	37.20	47.40	41.70
		RN101+FT	38.57	49.44	43.33	41.12	47.01	43.87
		RN50	33.33	41.87	37.12	33.99	42.71	37.86
		RN152	34.77	44.44	39.01	35.12	48.19	40.63
		GoogleNet	26.24	31.94	28.81	26.32	35.69	30.30
		VGG16	30.81	33.82	32.25	27.75	40.00	32.77
		Alexnet	22.64	25.76	24.10	16.09	38.75	22.73
		Shufflenet	31.55	36.39	33.80	29.03	39.44	33.45
		Inceptionv3	31.05	43.26	36.15	28.91	46.11	35.54
		Inceptionv3 _{adv}	31.43	44.37	36.80	35.12	38.54	36.75
	RN50-MOCO [†]	36.16	37.85	36.99	36.12	41.94	38.82	
	RN50-DINO [†]	40.54	49.24	44.47	42.95	50.07	46.23	
	MLP	MLP-Mixer	6.94	8.40	7.60	6.98	13.06	9.09
ViT	ViT _{large}	51.59	63.75	57.03	54.15	57.22	55.64	
	DeiT _{base}	31.94	45.69	37.60	36.98	43.54	39.99	
	ViTB16-DINO [†]	40.04	51.53	45.06	39.61	53.19	45.41	
I-21k	MLP	MLP-Mixer _{L16}	19.92	32.99	24.84	25.23	30.63	27.67
	ViT	ViT _{base}	51.63	55.56	53.52	52.29	55.90	54.03
		ViT _{large}	32.13	68.96	43.84	49.34	59.44	53.92
		ViT _{huge}	30.43	62.01	40.82	44.42	50.00	47.04
		ViT _{huge} +FT	39.53	47.99	43.35	44.57	52.22	48.10

Table 13. Results of Disentanglement Based Methods for the SUN dataset using different features extracted from a diverse set of architecture types pretrained on ImageNet-1k (I-1k) and ImageNet-21k (I-21k). These backbones were trained via: supervised and self-supervised ([†]) learning. The bold numbers correspond to the highest scores per column, and the shaded rows correspond to the most performant image feature per method. +FT indicates the features were fine-tuned with the seen classes from the training set. The most performant visual features are extracted from a ViT_{large} pretrained on ImageNet-1k using the SDGZSL method.

Disentanglement Based GZSL Methods								
AWA2 Dataset								
Dataset Pret. on	Arch Type	Backbone	SDGZSL			FREE		
			<i>Seen</i>	<i>Novel</i>	<i>Harm.</i>	<i>Seen</i>	<i>Novel</i>	<i>Harm.</i>
I-1k	CNN	RN101	75.27	58.65	65.93	75.22	56.00	64.20
		RN101+FT	83.99	60.35	70.24	87.66	47.56	61.67
		RN50	75.25	64.99	69.75	84.75	41.93	56.10
		RN152	79.08	68.38	73.34	86.78	50.13	63.55
		GoogleNet	71.62	54.53	61.91	72.03	49.45	58.64
		VGG16	78.12	57.02	65.93	76.39	54.86	63.86
		Alexnet	61.06	49.09	54.43	60.53	48.34	53.76
		Shufflenet	74.12	52.98	61.79	68.45	50.69	58.25
		Inceptionv3	84.46	57.82	68.65	84.40	43.32	57.26
		Inceptionv3 _{adv}	80.22	57.68	67.11	85.38	51.71	64.41
	RN50-MOCO [†]	66.26	48.95	56.31	72.37	48.88	58.35	
RN50-DINO [†]	68.56	64.99	66.73	74.89	52.41	61.67		
MLP	MLP-Mixer	31.69	25.2	28.07	28.29	22.66	25.16	
ViT	ViT _{large}	86.87	70.37	77.75	87.29	48.14	62.06	
	DeiT _{base}	80.13	56.06	65.96	72.55	41.13	52.50	
	ViTB16-DINO [†]	77.10	56.00	64.88	80.40	44.79	57.53	
I-21k	MLP	MLP-Mixer _{L16}	52.94	37.09	43.62	72.82	37.4	49.42
	ViT	ViT _{base}	88.00	60.76	71.88	77.14	48.44	59.51
		ViT _{large}	86.04	64.65	73.83	80.58	43.4	56.42
		ViT _{huge}	83.33	62.74	71.58	87.43	43.28	57.90
		ViT _{huge} +FT	76.94	58.43	66.42	82.36	43.10	56.59

Table 14. Results of Disentanglement Based Methods for the AWA2 dataset using different features extracted from a diverse set of architecture types pretrained on ImageNet-1k (I-1k) and ImageNet-21k (I-21k). These backbones were trained via: supervised and self-supervised ([†]) learning. The bold numbers correspond to the highest scores per column, and the shaded rows correspond to the most performant image feature per method. +FT indicates the features were fine-tuned with the seen classes from the training set. The most performant visual features are extracted from a ViT_{large} pretrained on ImageNet-1k using the SDGZSL method.

GZSL Methods using CLIP Visual Features																
Data Back set	bone	tfVAEGAN			CADA-VAE			SDGZSL			FREE			CE		
		Seen	Novel	Harm.	Seen	Novel	Harm.	Seen	Novel	Harm.	Seen	Novel	Harm.	Seen	Novel	Harm.
CUB	R50	66.91	49.96	57.20	61.67	56.67	59.06	61.24	56.89	58.98	62.95	47.70	54.28	40.72	37.32	38.95
	R101	65.83	60.13	62.85	62.31	61.97	62.14	65.03	59.53	62.16	59.41	60.05	59.73	60.00	52.52	56.01
	R50 _{x4}	70.48	65.41	67.85	67.90	68.84	68.37	66.38	67.77	67.07	68.55	59.75	63.85	62.57	44.50	52.01
	R50 _{x16}	73.94	69.22	71.50	76.40	67.15	71.47	72.65	68.92	70.74	71.02	63.27	66.92	61.04	46.26	52.63
	R50 _{x64}	82.09	67.93	74.34	75.91	70.84	73.29	74.77	73.70	74.23	68.53	<u>73.47</u>	70.91	59.06	49.52	53.87
	ViT _{B32}	64.37	62.08	63.20	64.34	57.52	60.74	64.20	59.66	61.84	61.51	54.87	58.00	60.96	50.55	55.27
	ViT _{B16}	76.48	66.32	71.04	71.13	67.79	69.42	64.81	<u>74.25</u>	69.21	68.46	65.99	67.20	58.30	<u>62.17</u>	<u>60.17</u>
	ViT _{L14}	<u>77.67</u>	<u>72.36</u>	<u>74.92</u>	<u>77.90</u>	<u>72.98</u>	<u>75.36</u>	<u>79.50</u>	73.49	<u>76.38</u>	<u>79.05</u>	65.38	<u>71.56</u>	<u>74.04</u>	46.38	57.03
	ViT _{L14} [†]	80.39	72.86	76.44	81.96	71.24	76.22	79.19	74.70	76.88	78.87	65.89	71.80	71.49	48.62	57.88
	ViT _{L14} [‡]	80.73	73.59	76.99	79.51	74.68	77.01	80.40	74.33	77.25	79.47	68.25	73.44	75.12	51.14	60.86
	ViT _{L14} [§]	82.82	72.27	77.18	81.47	75.05	78.13	80.38	75.67	77.96	80.48	67.54	73.45	71.15	56.82	63.18
	SUN	R50	51.94	53.40	52.66	47.87	61.88	53.98	43.29	54.10	48.10	53.10	54.24	53.66	38.84	52.85
R101		54.53	62.99	58.46	53.02	61.53	56.96	53.88	63.96	58.49	53.18	58.19	55.57	51.24	55.83	53.44
R50 _{x4}		54.38	65.00	59.22	55.16	60.56	57.73	55.00	65.62	59.84	53.37	62.57	57.61	54.92	55.07	55.00
R50 _{x16}		57.87	68.33	62.67	57.64	62.92	60.16	46.71	61.18	52.97	54.22	62.22	57.95	54.26	<u>60.21</u>	57.08
R50 _{x64}		57.21	<u>69.79</u>	62.88	59.46	65.63	62.39	57.17	66.60	61.52	<u>60.04</u>	57.78	58.89	50.04	59.10	54.19
ViT _{B32}		58.14	63.40	60.66	54.50	61.94	57.98	56.43	61.67	58.93	51.67	61.11	55.99	53.95	52.92	53.43
ViT _{B16}		57.98	67.01	62.17	54.69	62.08	58.15	57.40	<u>66.94</u>	61.81	54.38	59.93	57.02	55.12	56.94	56.02
ViT _{L14}		<u>59.84</u>	68.89	<u>64.05</u>	<u>62.11</u>	<u>63.40</u>	<u>63.18</u>	<u>63.57</u>	62.71	<u>63.13</u>	58.18	<u>62.71</u>	<u>60.36</u>	<u>60.16</u>	57.85	<u>58.98</u>
ViT _{L14} [†]		61.75	70.49	65.83	61.47	65.76	63.54	62.56	64.44	63.49	58.95	62.99	60.90	52.79	64.37	58.01
ViT _{L14} [‡]		60.93	67.08	63.86	57.95	68.19	62.65	60.08	67.15	63.42	58.37	62.43	60.33	56.78	64.03	60.19
ViT _{L14} [§]		62.25	70.03	65.91	58.91	66.74	62.58	60.70	67.50	63.92	58.72	63.61	61.07	59.65	60.90	60.27
AWA2		R50	72.02	60.31	65.65	80.99	61.30	71.14	77.72	57.66	66.21	80.03	55.17	65.31	78.84	45.19
	R101	71.94	64.79	68.18	85.25	59.34	70.87	80.29	68.78	74.09	78.64	59.11	67.49	76.61	62.34	68.74
	R50 _{x4}	83.93	<u>68.02</u>	75.15	80.71	<u>69.87</u>	77.02	82.23	68.39	74.67	83.30	57.29	67.89	81.46	61.03	69.78
	R50 _{x16}	86.48	66.49	75.18	89.35	65.88	77.30	84.24	<u>73.18</u>	<u>78.32</u>	83.09	60.13	69.77	83.13	66.83	74.09
	R50 _{x64}	89.69	68.21	77.49	90.54	63.75	75.81	78.67	69.07	73.56	<u>87.60</u>	61.04	71.95	89.95	63.33	74.33
	ViT _{B32}	84.24	62.41	71.70	80.53	65.35	73.90	84.33	62.43	71.75	74.01	57.13	64.48	78.91	62.86	69.98
	ViT _{B16}	87.80	66.56	75.72	90.56	65.44	75.80	86.87	66.59	75.39	77.05	61.58	68.45	84.02	66.92	74.50
	ViT _{L14}	<u>90.95</u>	69.50	<u>78.70</u>	<u>92.68</u>	68.14	<u>77.99</u>	<u>89.99</u>	68.76	77.91	81.10	<u>65.99</u>	<u>72.77</u>	<u>85.63</u>	<u>71.96</u>	<u>78.20</u>
	ViT _{L14} [†]	91.25	67.77	77.77	90.48	70.07	78.98	89.18	71.40	79.30	81.27	71.56	75.94	85.12	78.02	81.41
	ViT _{L14} [‡]	93.40	72.61	81.70	93.51	73.85	82.53	85.77	74.16	79.54	81.29	65.62	72.62	89.85	64.12	74.84
	ViT _{L14} [§]	89.62	73.56	80.80	93.35	68.14	78.78	91.50	70.33	79.54	81.53	69.84	75.23	90.78	67.96	77.73

Table 15. Results of Generative and Disentanglement Based Methods for the CUB, SUN and AWA2 datasets using different features extracted from different size and architecture of the visual head from diverse CLIP models (i.e., Resnet50 (R50) and Vision Transformer (ViT)). The three bottom rows per section correspond to fine-tuned features using sentences with: † the class names, ‡ the attributes, and § both class names and attributes. The bold numbers correspond to the highest scores per column, the underline numbers correspond to the highest scores using features not fine-tuned, and the shaded rows correspond to the most performant image feature per method over all. Surprisingly, the most performant method for all datasets correspond to a *generative* based method.